

THS MICHIGAN STATE UNIVERSITY LIBRARIES

4623

This is to certify that the

thesis entitled

Electron Nuclear Double Resonance Characterization of Plastocyanin

presented by

Matthew Paul Espe

has been accepted towards fulfillment of the requirements for

Masters degree in Chemistry

Major professor

Date 8/9/90



PLACE IN RETURN BOX to remove this checkout from your record. TO AVOID FINES return on or before date due.

DATE DUE	DATE DUE	DATE DUE

MSU is An Affirmative Action/Equal Opportunity Institution
c:\circ\distatus.pm3-p.1

# ELECTRON NUCLEAR DOUBLE RESONANCE CHARACTERIZATION OF PLASTOCYANIN

Ву

Matthew Paul Espe

**A THESIS** 

Submitted to
Michigan State University
in partial fullfillment of the requirements
for the degree of

**MASTER OF SCIENCE** 

Department of Chemistry

1990

#### **ABSTRACT**

# Electron Nuclear Double Resonance Characterization of Plastocyanin

## By

## Matthew Paul Espe

Electron nuclear double resonance (ENDOR) has been used successfully in obtaining structural insight into small complexes but its application to biological macromolecules has been limited. In this work the technique of ENDOR is developed so as to be useful in obtaining structural information on proteins. The protein under study, plastocyanin, was isolated from spinach.

By using the crystal structure for poplar plastocyanin the hyperfine coupling (hfc) constants for the protons near the copper site were determined. These calculated hfc constants were then compared to the experimental values in order to assign the ENDOR resonances.

The ENDOR spectrum of spinach plastocyanin consists of seven sets of resonances, four of which could be assigned. These assignments indicate that the protons are in a portion of the protein that is structurally very similar between the two species. The inability to assign the other three resonances indicates that there are some structural differences near the copper site.

#### **ACKNOWLEDGMENTS**

First, I would like to thank Dr. Chris Bender for all his help in maintaining the spectrometer and teaching me to use it correctly. I would also like to thank all the members of the lab who have assisted me in this project. Most importantly I want to acknowledge Dr. G.T. Babcock for all his spiritual and financial support.

# **TABLE OF CONTENTS**

	Page
LIST OF TABLES	v
LIST OF FIGURES	vi
INTRODUCTION	1
MAGNETIC RESONANCE THEORY	13
COMPUTER APPLICATIONS	29
RESULTS	34
EXPERIMENTAL	34
DISCUSSION	49
FUTURE WORK	53
APPENDIX A: SOURCE CODE OF TENSOR.FOR	55
REFERENCES	62

# **LIST OF TABLES**

		Page
Table 1	Bond lengths and bond angles from PROTIN and neutron diffraction for histidine and cysteine	30
Table 2	Input for TENSOR	33
Table 3	Parameters for simulating the EPR spectrum of spinach PCy	38
Table 4	Pairs of resonances from the ENDOR spectrum of spinach PCy	39
Table 5	Spin density distribution used in calculating hfc tensors	43
Table 6	Protons assigned to the ENDOR spectra and their complete hfc tensors	47

# LIST OF FIGURES

		Page
Figure 1	Energy levels of a Cu(II) ion at constant magnetic field. The four EPR transitions are indicated by the arrows	15
Figure 2	(a) A representation of the g-tensor axis system showing axial symmetry. (b) A similar representation of the Cu(II) hyperfine coupling tensor and its co-linearity with the g-tensor axis system	19
Figure 3	Computer generated EPR spectrum for a Cu(II) ion with parameters similar to PCy	20
Figure 4	Energy levels of a hydogen atom at constant magnetic field. Both the EPR and ENDOR resonances are displayed	22
Figure 5	(a) Observed lineshape for an axial hfc tensor. (b) Observed lineshape for a rhombic hfc tensor	24
Figure 6	<ul> <li>(a) EPR spectrum of PCy at 10 K. Conditions: microwave power, 2.07 mW; 12.5 KHz modulation amplitude, 0.4 Gpp; microwave frequency, 9.45543 GHz; sweep time, 200 sec.</li> <li>(b) Simulation of (a) using parameters in Table 3</li> </ul>	37
Figure 7	ENDOR spectra of PCy for the positions marked A, B, and C in Figure 6. Conditions: RF power, 90 W; modulation frequency, 40 KHz; microwave power, 20.7 mW; microwave frequency, 9.43556 GHz; sweep time, 200 sec	40
Figure 8	ENDOR spectra of PCy for the positions marked D and E in Figure 6. Conditions: same as in Figure 7	41

#### INTRODUCTION

Biophysics is a unique field of study in that it incorporates not only the areas of biology and biochemistry but also many areas of chemistry and physics. One of the most active areas within this field is the study of structure-function dynamics. That is, what particular structural characteristics of a biological species, such as a metalloprotein, correspond with biological functions. Whereas the biologist or biochemist can determine the composition of the species, such as number and type of amino acid and metal cofactors, and in some cases the location and function of these constituents, their techniques generally do not give direct information on the structure of the species.

With the use of a large variety of spectroscopic techniques though, a thorough description of biological macromolecules and their active sites can be obtained. Once the detailed picture of the active site in a protein has been produced, a study of structure-function relationships can be carried out.

Experiments can be done to determine what structural or electronic changes occur when the protein undergoes such biological activity as electron transfer, binding to substrates, or enzymatic activity. Environmental effects on the protein, such as changes in pH or temperature, can also be studied.

In the study of the metal sites in metalloproteins one area of extensive investigation is the location and catalytic relevance of nearby protons. These protons are well studied because of the wealth of physiological information that can be obtained. Such information includes the presence of hydrogen bonds, whether the system

under study is involved in proton pumping, structural changes that occur upon binding with substrates, and geometric and electronic structure at a metal site.

The work presented in this thesis describes the application of Electron Nuclear Double Resonance (ENDOR) in the study of protein structure, both geometric and electronic, at the copper containing metal site in the protein Plastocyanin (PCy). The work is aimed at providing information on the structural characteristics of the metal site, in particular on protons near the metal, and on the distribution of the unpaired electron spin density in PCy. In this case, methods that have been applied to the study of smaller molecules will be extrapolated to and tested to see if they are also applicable to the study of metalloproteins.

Plastocyanin from spinach (Spinacia oleracea L.) was chosen for this study for several reasons. First, PCy is a biologically interesting protein that is available in high purity and concentration. Also, the high resolution (1.8 Å) <sup>1</sup> crystal structure has been solved for the plastocyanin isolated from the closely related species, poplar. This allows comparison of the crystallographic data with the experimental magnetic resonance results. Last, the metal atom under study in PCy is copper, the properties of which make it ideally suited for ENDOR studies.

Plastocyanin is a member of a group of small, 10,000 to 25,000 Dalton, single-copper-containing proteins known as Type 1 or blue copper proteins (BCP). BCP were first discovered in 1958 and are found in bacteria where they are commonly called azurins, and in blue-green algae and higher plants where they are commonly called plastocyanins<sup>2</sup>. In all three groups the function of the protein is to mediate electron transfer between two other redox active species.<sup>3</sup>

The crystal structures of a higher plant BCP and two bacterial BCP have been resolved. 1,4,5 The crystal structure in each case showed that the copper atom is ligated to two nitrogens from histidines, the sulphur atom of cysteine, and the

sulphur atom of methionine. The metal site coordination geometry, which is nearly the same in all three proteins, is best described as a flattened tetrahedron.

The primary optical characteristic of BCP is an absorption maxima near 600 nm with an absorption coefficient of 3000-5000  $M^{-1}cm^{-1}$ , which gives the proteins their characteristic blue color. The EPR spectra of BCP also have several characteristic features that include axial or slightly rhombic spectra,  $g_{\parallel} > g_{\perp} > 2.00$ , and smaller than normal copper hyperfine coupling. The redox potential of BCP are spread over a wide range, from 184 mv to 390 mv, all of which are higher than that for tetraaquo Cu(II), which occurs at 153 mv.<sup>3</sup>

The function of the BCP in bacteria is not well understood except that they are electron transfer agents.<sup>3</sup> In higher plants the role of BCP is to mediate electron transfer from photosystem II (PSII) to photosystem I (PSI). PSII and PSI reside in the thylakoid membrane of the chloroplast whereas PCy, a water soluble protein, is loosely bound on the luminal side of the membrane. The role of PCy in photosynthesis is the transfer of electrons between cytochrome f in the cytochrome b6/f complex and the redox active chlorophyl complex in the reaction center in PSI.<sup>3</sup>

Many techniques have been used in the study of protein structures in metalloproteins. Each technique reveals unique pieces of information, the collective body of which produces much insight into the structure of the protein. Below is a brief description of several of the physical methods used to study PCy. Along with a discussion of the results obtained by each of the techniques is a consideration of its advantages and disadvantages.

### **Absorption Spectroscopy**

A large quantity of information on the metal sites in transition metal complexes can be obtained from absorption spectroscopy, particularly when used with the complementary techniques of circular dichroism and magnetic circular dichroism.<sup>6</sup> In this kind of study the metal d-d transitions are of greatest interest and usefulness. The number and energy of these transitions can reveal information that allows the assignment of the point group of the metal site.

Early work had indicated that the ligands in PCy are probably nitrogen and sulfur.<sup>7,8</sup> Studies of PCy have shown that the d-d transitions occur below 11,000 cm<sup>-1</sup>, which is quite low in comparison with most copper complexes with nitrogen and sulfur ligands.<sup>9</sup> The d-d transition energies for octahedral complexes with six nitrogen ligands have been reported in the range 13,400-14,300 cm<sup>-1</sup> and 17,100-17,500 cm<sup>-1</sup>.<sup>10</sup> The square pyramidal complex, Cu(NH<sub>3</sub>)5<sup>2+</sup>, has its transitions at 11,400 and 15,000 cm<sup>-1</sup>, which are still higher than PCy.<sup>10</sup> Spectra observed for square planar Cu(II)-amino acid complexes show d-d transitions in the ranges 15,400-17,700 cm<sup>-1</sup> and 17,500-20,600 cm<sup>-1</sup>.<sup>11</sup> Exchanging two sulfur ligands for two nitrogens, giving a N<sub>2</sub>S<sub>2</sub> donor set, shifts the energies to 13,000 and 21,000 cm<sup>-1</sup> for the square planer complex.<sup>12</sup> These results were used to rule out 5- and 6-coordinate and square planer 4-coordinate complexes as the coordination geometry for the metal site.

The exact geometry of the metal site can not be determined from the absorption spectra of PCy but the results allowed the elimination of many possibilities. The remaining possible geometries include trigonal 5- and 4-coordinate and distorted tetrahedral complexes. The ligands to copper are also not identified from these results but the low transition energies would indicate such ligands as nitrogen, sulfur, or oxygen. 13

#### **Electron Paramagnetic Resonance (EPR)**

EPR spectroscopy is useful in determining structure at the metal site as well as revealing insights into the ground electronic state of the metal site. EPR results can give information as to the type and number of ligands and the particular d orbital in which the unpaired electron resides. The EPR spectra of PCy are characterized by the following: a)  $g_{\parallel} > g_{\perp} > 2.0$ , b) axial or nearly axial g-tensor, and c) small copper hyperfine coupling (hfc) values. <sup>14</sup> The ordering and magnitude of the g tensor values are the most useful parameters in the spectroscopic determination of the metal site geometry.

Both 5- and 4- coordinate trigonal structures, dicussed above as possible geometries for the metal site in PCy, have the unpaired electron located in the  $d_z^2$  orbital. This electronic configuration typically gives g values that have  $g_{\parallel} \sim 2.0$   $< g_{\perp}$ , which are opposite to those seen for PCy. The PCy EPR spectra is consistent with the unpaired electron residing in a  $d_x^2$ -y orbital, which is the expected electronic ground state of a distorted tetrahedron. Attempts to fit the experimental g values with this geometry have produced good results.

The unusally small copper hfc constant, along with the lack of any other hfc in the ESR spectra, gives information about the distribution of the unpaired electron spin density about the metal site. In the case of Cu-EDTA, where the spin is located completely, or nearly completely, on the copper atom, A<sub>I</sub> is 588 MHz, compared to 180 MHz for PCy. The small value of A<sub>I</sub> in PCy indicates that a significant portion of the spin density is removed from the copper atom. Many inorganic copper complexes with nitrogen ligands show nitrogen hfc in their EPR spectra.<sup>20</sup> Since nitrogen hfc are not detected in PCy the amount of spin density delocalized onto the nitrogen ligands must be small. The unpaired spin must be located on atoms with zero nuclear spin since hfc from atoms other than copper are

not seen in the EPR spectra. Theoretical calculations indicate that a significant portion of the spin density (35 %) is delocalized onto the cysteine sulfur ligand.<sup>21</sup> Since <sup>33</sup>S (natural abundance 0.76%) is the only sulfur isotope with a nuclear spin, the exact spin density on the sulfur has not yet been determined.

EPR spectroscopy provides a qualitative indication of the delocalization of the spin density and has been used in conjunction with the analysis of the optical absorption spectrum to provide a good description of the geometry of the metal site. Providing detailed molecular structure from the results obtained with these methods has not been possible though, due to the low resolution of these two techniques. Hydrogen atoms, for example, are not resolved at all in the EPR spectra of PCy.

## X-Ray Absorption Spectroscopy

The methods of X-ray absorption spectroscopy (XAS) and extended x-ray absorption fine structure (EXAFS) have been used to provide extensive insight into metal site structure in metalloproteins. Information is contained in two regions of the x-ray absorption spectrum, the absorption edge and the EXAFS. The absorption edge reveals information on the oxidation state and site symmetry of the metal, and in some cases the type of liganding atoms. Typically however, edge data are only used to determine the oxidation state of the metal. The EXAFS spectra give more detailed insight, such as a more accurate prediction of ligand type, and interatomic distance between ligand and metal. EXAFS can still not tell the exact type of ligand atom but can limit it to an atomic weight range i.e. C,N, or O.

XAS results provide little information on the copper in PCy, showing only that the oxidized form of PCy contains copper in the +2 state.<sup>22</sup> A study of the reduced form of PC shows copper to be in the +1 state in this form of the enzyme,

supporting the fairly obvious conjecture that redox activity is mediated by the copper atom.

The EXAFS technique was first applied to azurin (Ps. aeruginosa) and the following results on the identity and distance of the nearest atoms to the copper were obtained: 2.6 atoms (N,O) at 1.97 Å, 1.3 S at 2.10 Å, and 0.6 S at 2.24 Å. <sup>23</sup> The second sulfur atom is not well detected and the distance determined is a best estimate. Except for the second sulfur atom, these results compare well with the crystal structure data, which indicate 2N at 2.11 Å, 1 S at 2.20 Å, and 1 S at 2.79 Å. <sup>4</sup> Similarily, a good correlation between the EXAFS results and the crystal structure was also seen for poplar PCy.<sup>24</sup> Again in this case the sulfur atom farthest from the copper could not be detected well and the possibility that there is a large error in this result was noted.

The application of XAS techniques both confirms previous data and provides new insight into the metal site geometry. The EXAFS data confirmed the type of atoms liganding to the copper as nitrogen and sulfur and provided information on the bond distances between the copper atom and its ligands. EXAFS does have some problem in determining the exact stochiometry of the liganding atoms as the azurin results show. Also, EXAFS seems to be limited in the amount of structural information it can provide as there are no reports of information on the positions of other atoms in BCP other than the ligands to the copper.<sup>22</sup>

#### X-Ray Crystal Structure

The techniques described above can give much information about the structure of metalloproteins but suffer from several important drawbacks. The results are either not completely specific-for example, EXAFS can only narrow the type of liganding atom to a small group-or the results must be interpreted in terms

of model compounds-as in the case for absorption and EPR spectroscopy. In order to obtain an accurate 3-dimensional structure of a protein, x-ray diffraction techniques must be used. X-ray crystallography, when used in conjunction with the amino acid sequence, can determine the position and type of each atom in the protein.

The crystal structure of oxidized PCy was determined first to 2.7 Å<sup>25</sup> resolution and later refined to 1.6 Å resolution. <sup>1</sup> At this level of refinement many of the ambiguities remaining for the metal site structure were resolved. The metal site in PCy was shown, as previously predicted, to be a modified tetrahedron. Previous studies of the metal site, though predicting N and S ligands, could not determine the exact number of each or if there were any other ligands to the metal. The crystal structure resolved the uncertainty in the nature of the liganding atoms by showing that there were only four ligands to copper, 2 N and 2 S. The crystal structure also showed that there were no water molecues at the copper site and none within the protein.

The distorted tetrahedral geometry of the metal site in PCy is unusual for copper complexes. Further crystallographic work has shown that this geometry is the result of the polypeptide. Comparison of the crystal structure of the apoprotein (1.8 Å resolution) <sup>26</sup> with that of the oxidized form shows only small differences near the copper site. The crystal structure has also been determined for the reduced form of PCy<sup>27</sup> as well as for the Hg(II) substituted protein<sup>28</sup>. In each case only small structural differences are seen near the copper site. The polypeptide thus provides the optimum geometry for the metal site to facilitate electron transfer most effectively.

X-ray diffraction methods provide a wealth of data but also suffer from several drawbacks. First, in order to study a protein, a single crystal must be grown. In the case of BCP many species were attempted until PCy from poplar was

crystallized. Second, the crystal structure determined is a static description of the protein. Studies of the structure of the protein under different conditions, such as in different oxidation states, at different pH values, or interacting with other systems, require a single crystal be grown under each new condition. This has been done for PC at different pH<sup>27</sup> values but could prove to be very difficult or impossible for PCy-redox partner systems. Techniques are needed that are capable of studing protein structure in liquid and frozen solutions that allow comparison of the results with the crystal structure.

## **Nuclear Magnetic Resonance (NMR)**

NMR has been used in the solution study of many aspects of protein structure and dynamics. Metal binding site characteristics<sup>29</sup>, interaction sites of redox partners<sup>30</sup>, and global structure<sup>31</sup> have all been studied in PCy by NMR. NMR titration experiments of the histidines in PCy showed that their pKa values shift from their normal values of around seven to five, indicating that these amino acids are ligands to the metal.<sup>7</sup> Substitution of <sup>113</sup>Cd for copper in BCP followed by <sup>113</sup>Cd NMR provided qualititive information on the metal binding site.<sup>29</sup> The <sup>113</sup>Cd chemical shift for azurin is significantly different from that of PCy. This indicated that the copper sites in these two BCP are different. The refined crystal structure of azurin (Alcaligines denitrificans)<sup>5</sup> showed that it may also have a long copper-oxygen bond, in addition to the long copper-sulfur bond.

The most important advance in NMR studies of relatively low molecular weight, soluble proteins is the ability of the technique to determine the complete 3-dimensional structure.<sup>32</sup> With the use of a variety of pulse sequences and muti-dimensional techniques that are now available, nearly every proton in a low molecular weight protein can be assigned. These assignments, in conjunction with

NOE studies, which give relative distances between protons, and distance geometry algorithms allow the tertiary structure of the protein to be determined.<sup>32</sup> A complete assignment has been carried out for both French bean<sup>31</sup> and spinach PCy<sup>33</sup> and for French bean the tertiary structure has also been obtained. The overall solution structure is similar to the crystal structure for poplar PC, but there are some local differences.<sup>31</sup>

Even though NMR can be used to obtain the tertiary structure of a protein, there are some limitations. With proteins comparable in size to PCy the proton NMR spectra become very complex and a complete assignment of the spectra is difficult and time-consuming. The assignment of the spectra for PCy required the application of a large number of NMR techniquies. So far the largest protein to be completely mapped out is French bean PCy which contains only 99 amino acids. This technique then is currently limited only to the study of those metalloproteins that are no larger than PCy.

#### **Electron Nuclear Double Resonance (ENDOR)**

Many of the biological systems under study have not yet been crystallized and thus the crystal structures are not known. Except for NMR, none of the methods discussed above is able to resolve spatial coordinates for protons near a metal site in a metalloprotein in solution. ENDOR, as for NMR, is a method well-suited for the study of soluble proteins that contain paramagnetic metals. Besides being able to study proteins in solution ENDOR also has several other advantages. It has been shown in previous experiments on organometallic compounds that metal-proton distances determined by ENDOR are accurate to 0.1 Å. <sup>34</sup> ENDOR can also be used to study all nuclei within a system that have a net nuclear spin. This would include H, N, P, and many transition metals. ENDOR can also be used to obtain

information on the ground electronic state of the metal. In particular, it can be used to determine whether the unpaired spin is isolated on the metal atom or distributed onto the protein ligands.

ENDOR, as with the other techniques, has its limitations and difficulties. In order to detect ENDOR resonances the nuclear relaxation times must be slowed down sufficiently to allow them to compete with the electronic relaxation times.<sup>35</sup> Achieving this condition for transition metal complexes requires cooling the sample to 20 K or lower. This necessitates the use of a liquid helium cooling system. The generally low concentration of isolated proteins, along with the small sample volumes, results in a very low concentration of paramagnetic centers. This low concentration, together with the inherent weakness of ENDOR signals, results in signal to noise ratios that are often quite low.

Unlike NMR the complete tertiary structure of the protein can not be determined from the ENDOR results. ENDOR can only be used to study that portion of the protein that is within approximately 8 Å of the paramagnetic site. Even though the entire protein can not be studied by ENDOR this technique has an advantage in that it looks fairly specifically at the active site. The spectra, then, are easier to interpret and do provide detailed structural information. With the simpler spectra, structural changes that occur near the active site under different conditions can be easily detected. ENDOR, then, is a technique that is very capable of addressing the questions raised at the beginning of this chapter.

Whereas ENDOR has been used successfully in obtaining structural insight into small organometallic complexes, <sup>34,36,37</sup> its application to biological macromolecules has been limited. In this work the ENDOR technique used to study inorganic complexes is developed so as to be useful in obtaining structural information on proteins such as PCy. Previous ENDOR work on BCP has concentrated only on the nitrogen ligands and those protons with strong isotropic

couplings.<sup>38,39</sup> Study of the much weaker dipolar interactions can be used to provide insight into the structure of the protein farther from the paramagnetic center than previously possible. PCy was chosen for this study for two reasons. First, since the crystal structure has been solved, the structural information determined by ENDOR can be compared with the crystallographic data. Second, for PCy biological approaches such as biosynthesis and molecular biology can be applied to help in the interpretation of the ENDOR results.

In the chapters that follow, the application of ENDOR to PCy is described in detail. In chapter 2 the theory that underlies the EPR and ENDOR experiments is discussed. This is followed by an introduction into the computer techniques used to help make assignments within the ENDOR spectra and determine structral information about PCy. Finally in chapter 4 the results obtained about the structural and electronic environment around the copper site in PCy are displayed and discussed.

#### MAGNETIC RESONANCE THEORY

EPR and ENDOR spectra are interpreted with the use of a spin Hamiltonian. This Hamiltonian acts upon spin-only wave functions and predicts their energies for the particular system under study. Allowed transitions between these energy levels can be induced by electromagnetic radiation of the appropriate frequency. The resonances present in EPR or ENDOR spectra represent the transitions between these energy levels. The Hamiltonian for EPR and ENDOR that is applicable for frozen solution samples of Cu(II) complexes is discussed in this chapter.

#### **EPR**

The Hamiltonian that describes the EPR spectral characteristics is:<sup>40</sup>

$$\mathcal{H} = \beta_{e} \mathbf{H} \mathbf{g}^{T} \cdot \mathbf{S} - \mathbf{g}_{N} \beta_{N} \mathbf{H} \cdot \mathbf{I} + \mathbf{S} \cdot \mathbf{A}^{T} \cdot \mathbf{I}$$
 (1)

H = Hamiltonian operator

 $g^{T}$  = electron g-tensor

 $\beta_e$  = electron Bohr magneton

 $g_N = nuclear g value$ 

 $\beta_N$  = nuclear Bohr magneton

H = Zeeman field (externally applied magnetic field)

A<sup>T</sup> = hyperfine coupling tensor

S = electron spin angular momentum operator

I = nuclear spin angular momentum operator

The first term of the equation, the electron-Zeeman term, describes the interaction between the unpaired electron and the externally applied magnetic field (Zeeman field). The effect of this interaction is to split the degeneracy of the two spin-only wavefunctions for the unpaired electron. This splitting, the Zeeman splitting, is the largest interaction of the unpaired electron in a Cu(II) complex and is diagrammed in Figure 1. Since the electron-Zeeman term is a function of the g-tensor its magnitude will be orientationally dependent and thus anisotropic. That is, the magnitude of this interaction will depend on the direction of the Zeeman field relative to the g-tensor. The g-tensor is diagonal in at least one coordinate system and this coordinate system will be the primary axis system used in the discussion of EPR and ENDOR.

The second term in equation 1 is the nuclear-Zeeman term which represents the interaction between the nuclear spin and the Zeeman field. This term is non-zero only for those nuclei that have non-zero nuclear spin. Unlike the electron-Zeeman term the nuclear g value is taken as isotropic. The nuclear-Zeeman interaction is directly analogous to the electron-Zeeman interaction except that in this case the degeneracy of the nuclear spin wavefunction is split. The splitting of the two wavefunctions is the nuclear-Zeeman splitting and is shown in Figure 1.

The third term in equation 1 describes the interaction between the unpaired electron and non-zero spin nuclei. This interaction is referred to as the electron-nuclear hyperfine coupling (hfc). For many Cu(II) complexes, including PCy, the only hyperfine coupling seen in the EPR spectra is to the nucleus of the copper atom. The hfc term is comprised of two components, equation 2, the orientationally independent (isotropic) Fermi contact coupling and the orientationally dependent dipolar coupling. The dipolar coupling is described by the tensor T and the Fermi

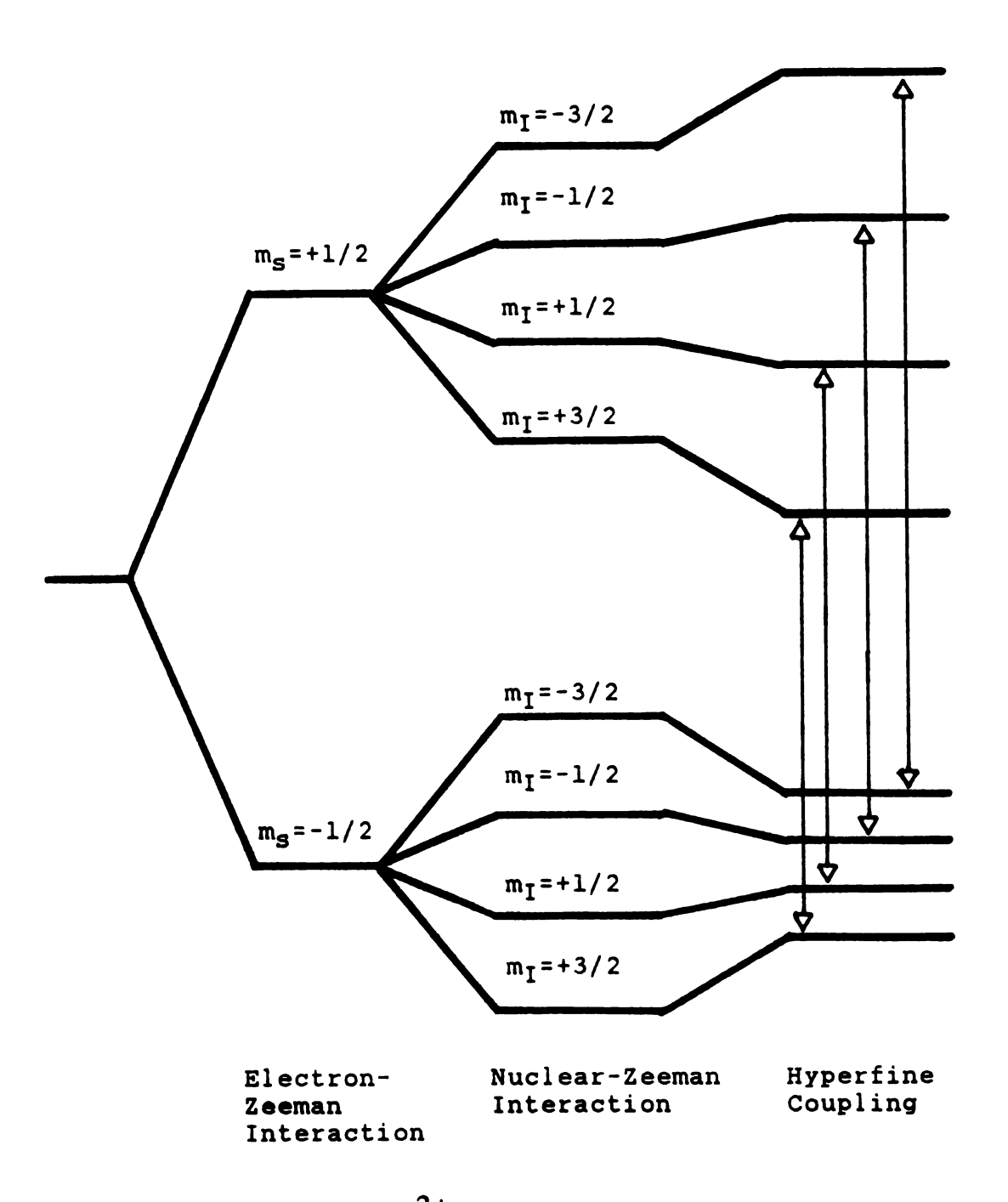


Figure 1 Energy levels of a Cu<sup>2+</sup> ion at constant magnetic field. The four EPR transitions are indicated by the arrows.

contact coupling by the scaler quantity a. The total coupling is the sum of the two components.

$$S \cdot A^{T} \cdot I = a(S \cdot I) + S \cdot T^{T} \cdot I$$

$$= A_{iso} + A_{Dip}$$
(2)

Fermi contact coupling results from unpaired spin density being located at the nucleus of the coupled atom, equation 3-a. In order for the unpaired spin density to be at the nucleus of the atom it must be located in an s orbital. The coupling of the unpaired electron to the copper nucleus in copper (II) complexes shows an isotropic component. Spin polarization by the unpaired electron in the 3d orbital causes unpaired spin density to reside in the inner shell s orbitals of the copper atom resulting in the Fermi contact coupling. Spin polarization by the unpaired electron can also cause unpaired spin density at the nucleus of atoms bonded to the atom containg the unpaired electron.

The dipolar coupling is a through space interaction between the unpaired electron and neighboring nuclei, equation 3-b. In the Cu(II) ion case, along with the Fermi contact coupling described above, there is also a dipolar coupling between the unpaired electron and the copper nucleus. Since the dipolar coupling is described by the tensor T it is anisotropic and the magnitude of the hfc tensor A is dependent on the orientation of the Zeeman field relative to the A-tensor axis system. The effect of the hfc on the energy of the wave functions is shown in Figure 1.

$$A_{iso} = 3\pi g_e \beta_e g_N \beta_N \Psi |(0)|^2 S \cdot I \qquad (3-a)$$

 $\Psi | (0) |$  = wavefunction evaluated at the nucleus

$$A_{Dip} = g_e \, \beta_e g_N \beta_N (3\cos^2\theta_{A^-} 1)/r^3 \qquad (3-b)$$

 $g_N = nuclear g-value$ 

 $\beta_N$  = nuclear Bohr magneton

r = magnitude of vector r between the electron spin and nuclear spin

 $\theta_A$  = angle between r and the Zeeman field

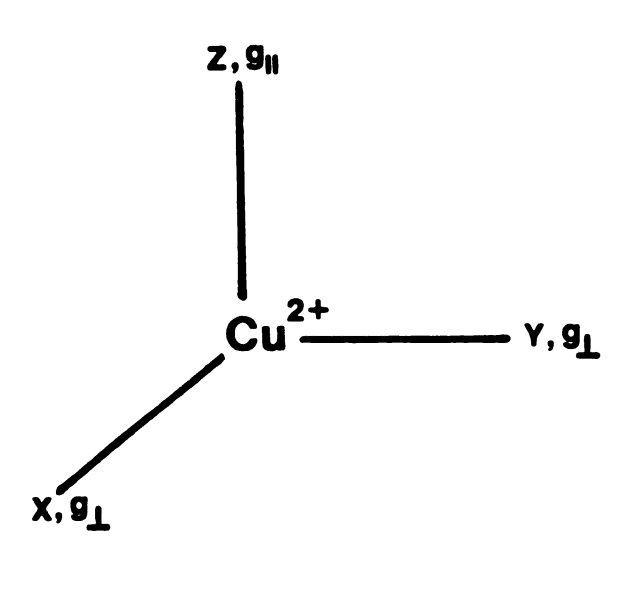
In the X-band EPR study of Cu(II) complexes it is assumed that the high field approximation is applicable. <sup>40</sup> In this approximation both the unpaired electron spin and the nuclear spins are quantized along the Zeeman field. In this case "sharp" eigenvalues are obtained from the spin operators S and I acting on the spin only wavefunctions. The eigenvalues obtained from these operators are the spin angular momentum in the direction of the Zeeman field. Under these conditions the scalar quantities,  $m_S$  and  $m_I$ , can be substituted for the operators S and I in the Hamiltonian, equation 1. A Cu(II) ion with one unpaired electron and a nuclear spin of 3/2 will have  $m_S = \pm 1/2$  and  $m_I = \pm 3/2$ ,  $\pm 1/2$ , depending on the electron and nuclear spin states.

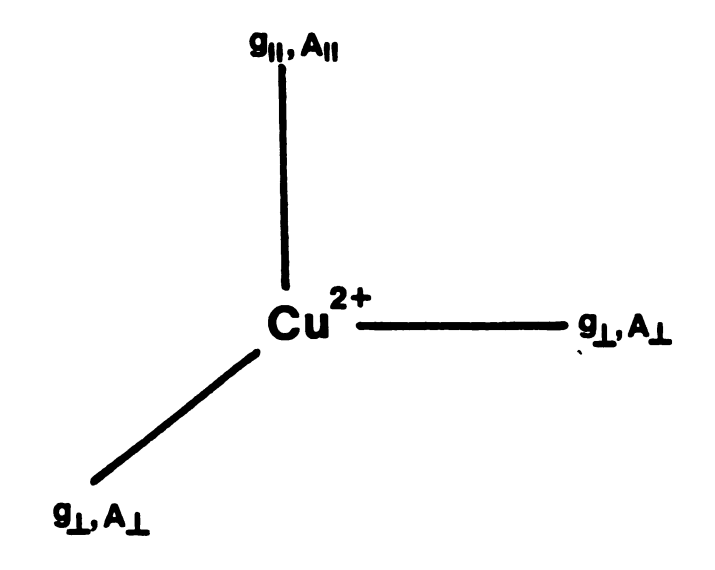
In the EPR experiment the selection rules are  $\Delta m_I = 0$ ,  $\Delta m_S = 1$  and the allowed EPR transitions are labelled in Figure 1. In an EPR transition the electronic spin undergoes a "spin flip" resulting in a one quantum change in the spin angular momentum. The energy of such transitions usually fall in the microwave frequency range. These transitions are detected in the EPR experiment and show up as peaks in the EPR spectrum.

The dominant features of the EPR spectra of frozen solution samples of Cu(II) complexes are dictated by the g- and copper hfc tensors. The g-tensor for

many copper complexes is axial, that is  $g_X = g_y = g_\perp$  and  $g_z = g_\parallel$ , where  $g_X$ ,  $g_y$ , and  $g_Z$  are the principal values of the g-tensor. If the unpaired electron is located in the  $d_X 2 - \gamma 2$  orbital of copper then the x and y axis of the tensor are located in the plane of this orbital and the z axis is perpendicular to this plane. In this electronic configuration the the g-tensor axis system and the frame of reference of the d-orbitals are colinear, Figure 2. The hfc tensor for coupling to the Cu nucleus in copper complexes also is axial in many cases. Similar to the g-tensor,  $A_X = A_y = A_\perp$  and  $A_Z = A_\parallel$  where  $A_X$ ,  $A_y$ , and  $A_Z$  are the principal components of the hfc tensor. The hfc tensor is also closely related to the geometry of the metal d orbitals and in many cases is colinear with the g-tensor, Figure 2.

In frozen solution samples of Cu(II) complexes the molecules are oriented in all possible directions. Each molecular orientation relative to the Zeeman field will have a scalar effective value for the g and hfc- tensors which are labelled geff and Aeff. Substitution of these effective values into the spin Hamiltonian results in a different EPR spectrum for each molecular orientation. The experimentally detected EPR spectrum is then a composite of the individual spectra and is referred to as a powder pattern spectrum. Figure 3 is a computer generated powder pattern EPR spectrum of a Cu(II) ion characteristic of a BCP. The primary feature in the spectrum is the copper nuclear hyperfine coupling. Since copper, nuclear spin 3/2, has four nuclear spin states, there are four hyperfine manifolds in the EPR spectrum. The splitting of these manifolds is dictated by the hfc tensor. The low field portion of the spectrum corresponds to those molecules oriented with their zaxis aligned along the Zeeman field,  $g=g_{\parallel}$ . The hyperfine coupling for this orientation is  $A_{\parallel}$  and the hyperfine manifolds are centered about  $g_{\parallel}$ . Similarly, the high field portion of the spectra corresponds to those molecules oriented such that the Zeeman field is in the molecular x,y plane. The hyperfine coupling is then  $A_1$ 





a) A representation of the g-tensor axis system showing axial symmetry. b) A similar representation of the Cu(II) hyperfine coupling tensor and its co-linearity with the g-tensor axis system.

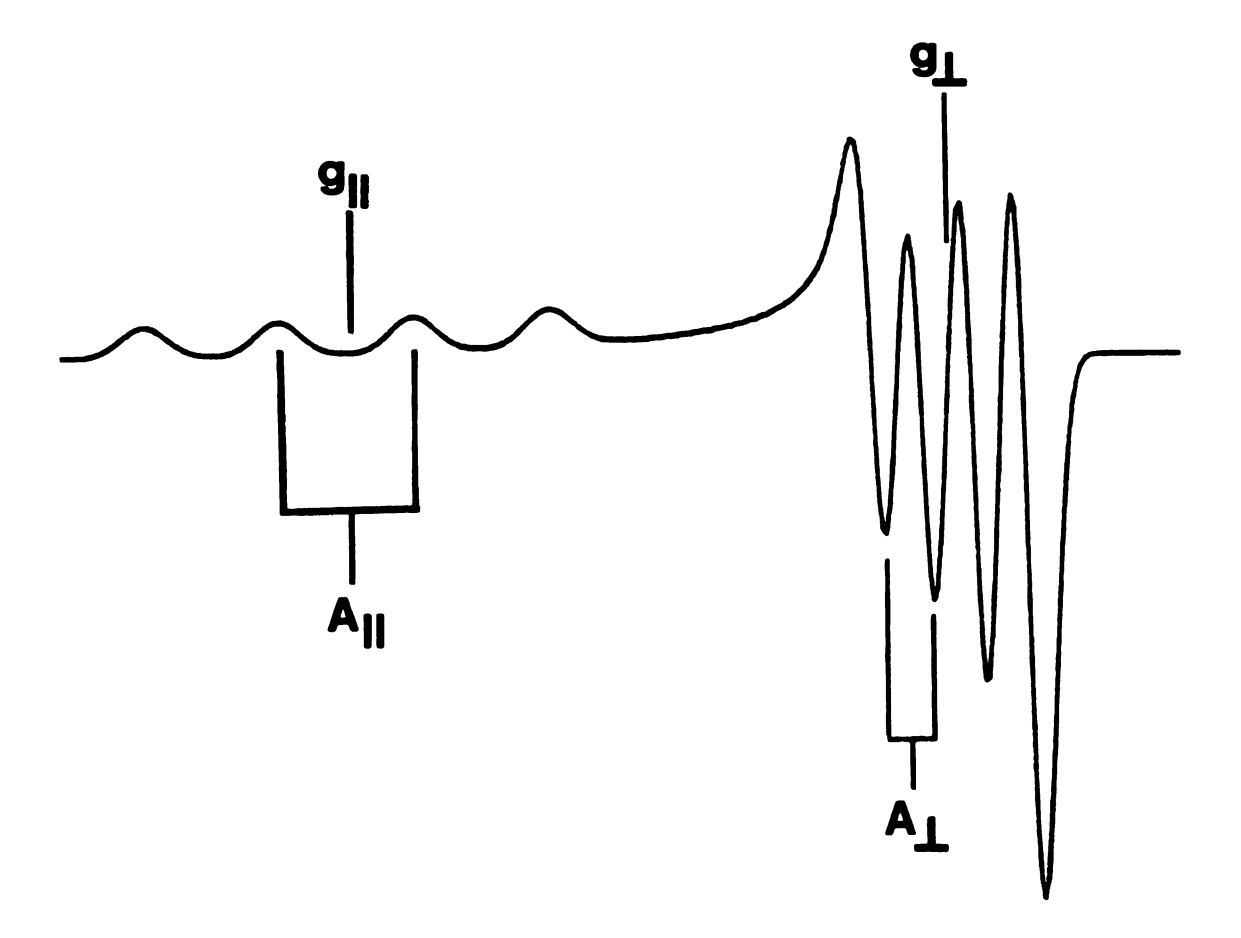


Figure 3 Computer generated EPR spectrum for a Cu(II) ion with parameters similar to PCy.

and centered about  $g_{\perp}$ . The powder pattern spectrum, Figure 3, clearly shows the orientational effects of the g and copper hfc tensors.

Besides hyperfine coupling to the copper nucleus there is also coupling between the unpaired electron and other nearby nuclei. The nuclei of interest in this work are the protons surrounding the metal site. These protons are generally not detected in the EPR spectra of Cu(II) complexes since their hyperfine coupling constants are very small compared to the large linewidth of the copper hyperfine coupling manifolds. In order to investigate these smaller hyperfine interactions a more sensitive technique with narrower linewidth is needed. ENDOR is well-suited for the study of these interactions.

#### **ENDOR**

The Hamiltonian that describes the ENDOR experiment is exactly the same as the one used for EPR.<sup>35</sup> Since the Hamiltonian is the same in both experiments the energy levels are also the same for the system under study. The difference in the two experiments is that the ENDOR experiment promotes and detects transitions between nuclear spin states rather than between electronic spin states as in EPR.

In discussing the ENDOR experiment we shall consider the case of an unpaired electron interacting with a single proton. This is the type of interaction that is detected when ENDOR is used to study PCy. The hyperfine coupling to the proton is described in equation 3. The energy level for this system is shown in Figure 4. Transitions between energy levels 1 and 3 and energy levels 2 and 4 are the EPR transitions. In the ENDOR experiment the selection rules are  $\Delta m_1 = 1$ ,  $\Delta m_S = 0$  and the system under study undergoes a nuclear spin flip. The ENDOR transitions then are between energy levels 1 and 2 and between energy levels 3 and 4. The splitting of these energy levels falls in the radiofrequency range. In

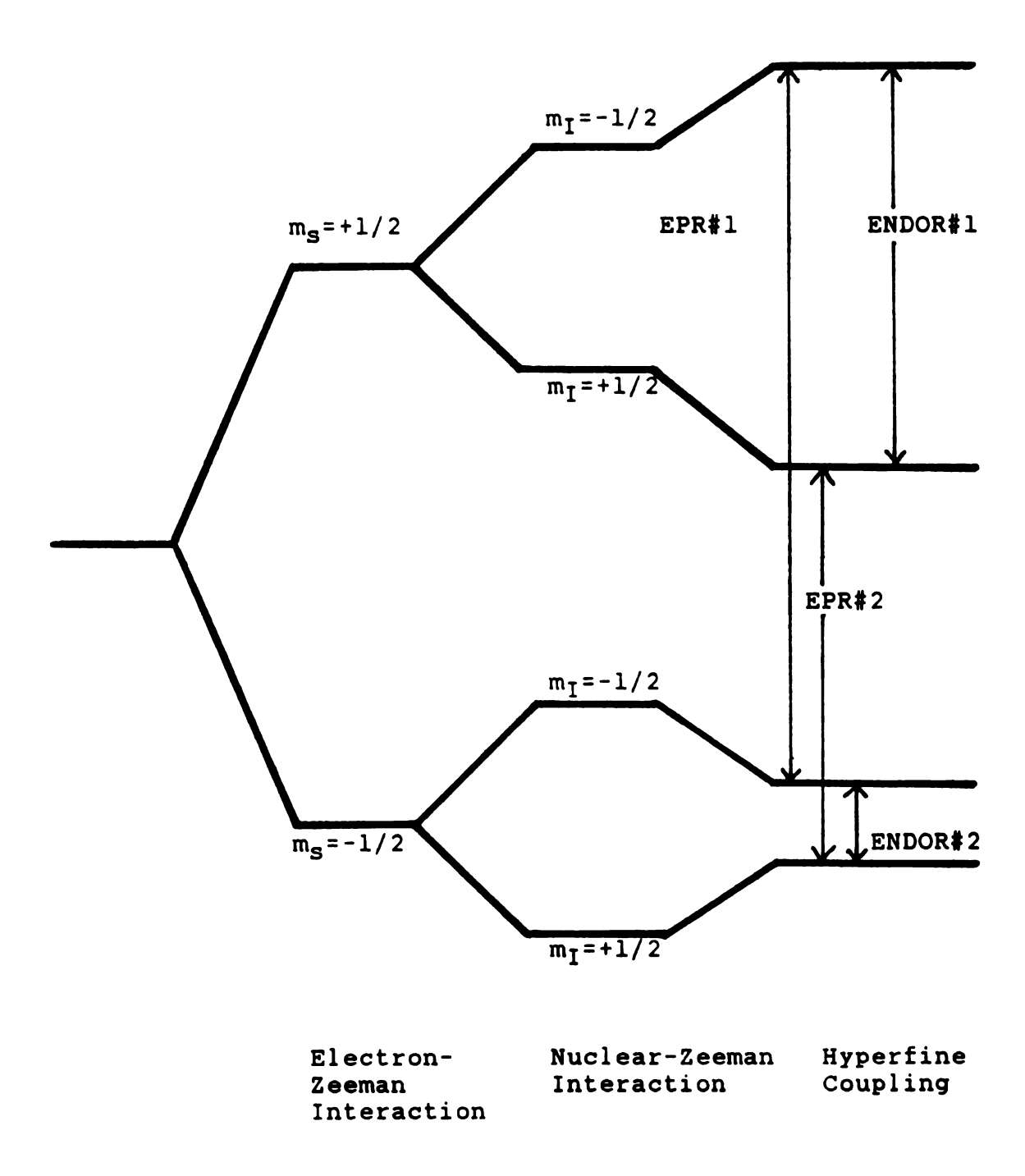


Figure 4 Energy levels of a hydrogen atom at constant magnetic field. Both the EPR and ENDOR transitions are displayed.

ENDOR, unlike EPR, the effect of the RF radiation on the EPR resonances are detected rather than direct detection of the absorption of RF power at frequencies corresponding to ENDOR#1 and ENDOR#2.

The Zeeman field strength is adjusted so that one of the EPR transitions, EPR#1, is in resonance. The microwave power is then increased to partially saturate this EPR transition. This has the effect of equalizing the populations of energy levels 2 and 4. The system is next irradiated with a swept radiofrequency. When the frequency of the RF fulfills the resonance condition of ENDOR#1, the transition will be saturated and the population of energy levels 3 and 4 will be equalized. This results in a lowering of the population of level 4 and a desaturation of the EPR#1 transition. The EPR transition will then increase in intensity and this change in intensity is detected as a peak in the ENDOR spectrum. A second ENDOR peak is detected when the RF fulfills the resonance condition for the ENDOR#2 transition. The ENDOR spectrum is, thus, simply the change in EPR intensity plotted as a function of RF frequency.

The ENDOR spectrum for this system consists of two peaks centered at  $\nu_N$  the free proton resonance.  $\nu_N$  is equal to the nuclear-Zeeman splitting, Figure 4. The splitting between the ENDOR resonances is A, the value of the hfc tensor for a particular molecular orientation. The energy at which the two ENDOR peaks will occur is predicted by equation 5,

$$h\nu = \nu_N + |A/2| \tag{5}$$

The ENDOR spectra of a spin system in a frozen solution will have distinct features depending on whether the hfc tensor is axial  $(A_x = A_y = A_z)$  or rhombic  $(A_x = A_y = A_z)$ . The lineshape that appears for an axial hfc tensor, shown in Figure 5, is comprised of a pair of absorptive shaped peaks and a pair of derivative shaped peaks.<sup>41</sup> For a hfc tensor that is purely dipolar, equation 3 predicts that  $A_{\parallel}$ , with

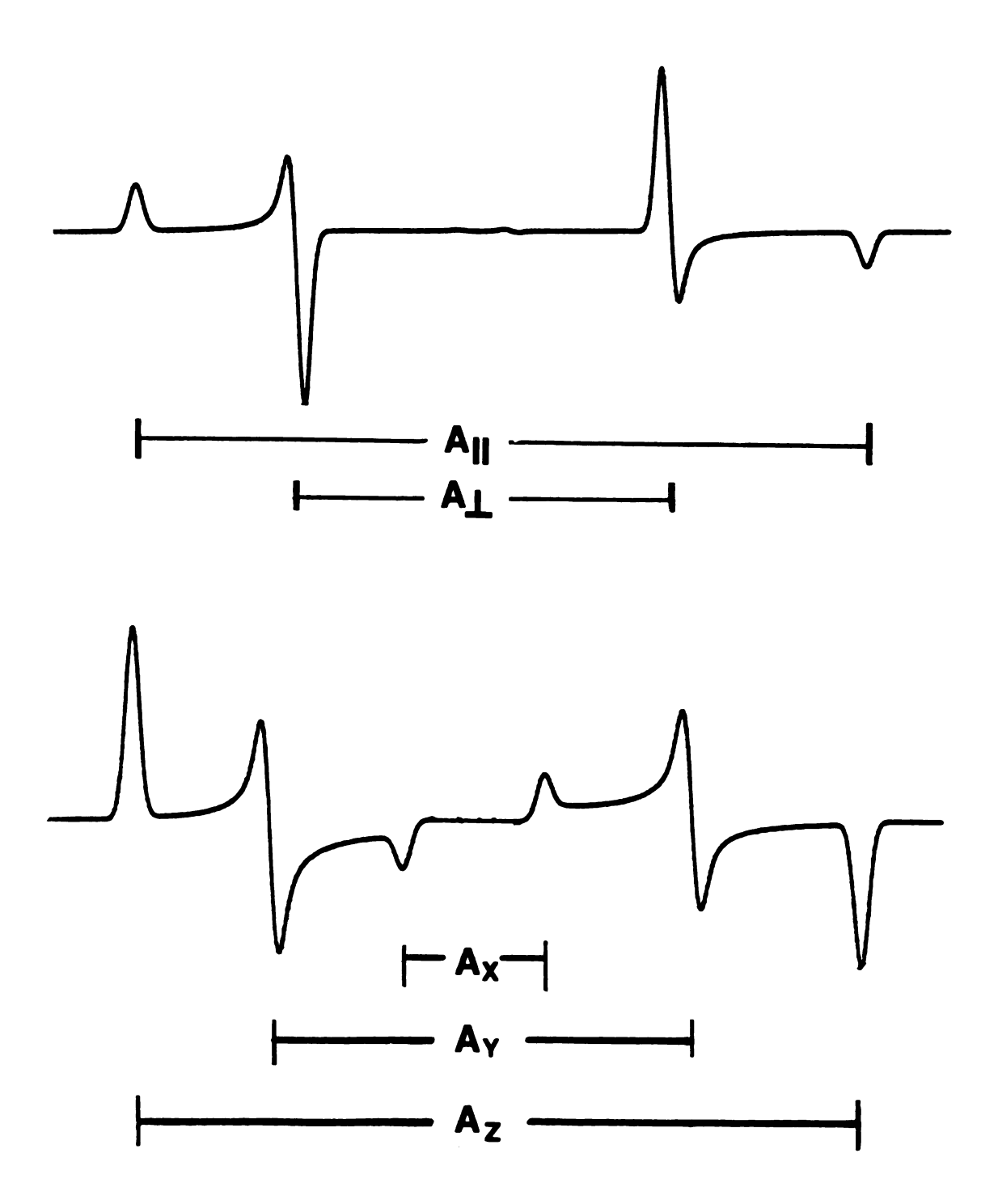


Figure 5 a) Observed lineshape for an axial hyperfine coupling tensor. b) observed lineshape for a rhombic hyperfine coupling tensor.

 $\theta_A=0^{\circ}$ , will be twice as large as  $A_{\perp}$  with  $\theta_A=90^{\circ}$ . The absorptive shaped peaks are then split by an amount equal to  $A_{\parallel}$  and the derivative shaped peaks by  $A_{\perp}$ . The lineshape for a rhombic hfc tensor is shown in Figure 5. The absorptive shaped peaks are split by  $A_z$ , the derivative peaks by  $A_y$ , and the rhombic shaped peak by  $A_x$ , where  $A_z > A_y > A_x$ .

#### Structural Information

In the previous section the values of g and A were shown to be a function of the angle beween the Zeeman field and the z-direction of their respective tensors. In the case of a spin system with axial tensors the scalar quantity of these tensors for a particular molecular orientation are described by equation 6,<sup>42</sup>

$$g_{\text{eff}} = (g_{\perp}^{2} \sin^{2}\theta_{H} + g_{\parallel}^{2} \cos^{2}\theta_{H})^{1/2}$$

$$A_{\text{eff}} = (A_{\perp}^{2} \sin^{2}\theta_{A} + A_{\parallel}^{2} \cos^{2}\theta_{A})^{1/2}$$
(6)

The angle  $\theta_H$  is the angle between the Zeeman field and  $g_{\parallel}$  for the g-tensor and  $\theta_A$  is the analogous angle for the A-tensor. Using the Cu(II) ion as an example, Figure 2, the value of the g-tensor when the Zeeman field is along the atomic z-direction,  $\theta_H = 0^{\circ}$ , is  $g_{\parallel}$  and when the Zeeman field is along the x-direction,  $\theta_H = 90^{\circ}$ ,  $g = g_{\perp}$ . In between these two extrema the value of g is determined from equation 5.

The situation is quite different for the A-tensor. Experimentally it is observed that the effect of changing  $\theta_A$  is not to change the value of A as in the g-tensor case but its effect is to modulate the intensity of the peaks in the ENDOR spectra. When the Zeeman field is along the z-direction of an axial A-tensor,  $\theta_A = 0^{\circ}$ , a pair of absorptive shaped peaks are detected with a coupling of  $A_{\parallel}$  and

when the Zeeman field is in the x,y plane,  $\theta_A = 90^{\circ}$ , a pair of derivative shaped peaks are detected with a splitting of  $A_{\perp}$ . As  $\theta_A$  increases from  $0^{\circ}$  to  $90^{\circ}$ , the intensity of the peaks separated by  $A_{\parallel}$  will decrease while at the same time the intensity of the peaks separated by  $A_{\perp}$  will increase. Regardless of the value of  $\theta_A$  no additional peaks will appear in the ENDOR spectra from the proton.

In the spin system of study in this work, PCy, the hfc tensors are not axial but rhombic. The change in ENDOR peak intensity for a rhombic hfc tensor is a straightforward extension of the axial case. The only difference is that a rhombic lineshape, Figure 5, will be detected. The intensity of these peaks will change as the Zeeman field is more closely aligned along or farther away from the principal directions of the hfc tensor just as for an axial hfc tensor.

The angles  $\theta_A$  and  $\theta_H$  can be changed by taking ENDOR spectra at a series of Zeeman field values within the EPR spectra. As ENDOR spectra are aquired at increasing Zeeman field, increasing  $\theta_H$ , each spectra will correspond to a different value of  $\theta_A$ . Correlation of the lineshape of the ENDOR peaks-absorptive, derivative, or rhombic-with their change in intensity allows an assignment of the peaks corresponding to a particular proton. Knowing the principal values of the hfc tensor and using equation 3 for hyperfine coupling the distance r between the unpaired electron and the proton is determined. Also, following the intensity changes of the ENDOR peaks versus  $\theta_H$  give an approximate angle between the vector r and the direction of  $g_{\parallel}$ . This angle, along with the distance to the proton, gives an accurate description of the position of the proton relative to the metal atom.

Application of the technique of "angle selection" ENDOR on compounds ranging from simple organics to organometallic complexes has provided a wealth of information. With the use of ENDOR spectroscopy the molecular geometry of the spin label 2,2,5,5,-tetramethylpyrroline-1-oxyl-3-carboxylic acid in a frozen solution

was determined.<sup>43</sup> Comparison of the ENDOR results with those obtained from crystal structures and molecular modeling showed only a 5% discrepancy in the structure of the compound.

Several groups have also used this technique to study the planar complex bis(acetylacetonato) copper (II) (Cu(acac)<sub>2</sub>).  $^{36,44}$  The difference between the experimentally determined proton hfc tensors for a frozen solution sample and single crystals was minimal. The hfc tensors from a powdered crystal, where copper has been doped into crystals of Pd(acac)<sub>2</sub>, also compared well with those from single crystals. The powdered crystal sample also showed two additional pairs of ENDOR peaks not detected with the frozen solution sample. These peaks result from the interaction of the unpaired electron on the copper atom with the methylene proton on a neighboring Pd(acac)<sub>2</sub> molecule. This coupling was purely dipolar and the the magnitude of the two couplings were A<sub>1</sub> and A<sub>1</sub>. By using these couplings along with the formula for dipolar coupling the distance from the metal atom to the proton was determined. Comparison of this distance with the distance calculated from the crystal structures of Cu(acac)<sub>2</sub> and Pd(acac)<sub>2</sub> showed good agreement.

This technique has also been extended to study non-planar organo-metallic complexes. The ligand environments around the Gd<sup>3+37</sup> and VO<sup>2+34</sup> ions have been studied in frozen solutions of methanol or methanol/water cosolvent. The ENDOR results revealed insight into the ligand geometry along with the type of ligand, CH<sub>3</sub>O<sup>-</sup>, HO<sup>-</sup>, or H<sub>2</sub>O, and to some extent, their stochiometries. Ligand geometries determined by ENDOR were very close to those from crystal structures of similar compounds.

In the work cited above the unpaired electron is localized on the metal atom or in the spin label system roughly half way between the N and O of the nitroxide group. As discussed above this is not the situation for PCy, where a portion of the

unpaired spin density is delocalized onto several of the liganding atoms. The angle selection technique is still applicable for this system but structural information for protons nearby the metal atom can not be calculated from the hfc tensor in a straightforward manner. When the unpaired spin density is delocalized over several atoms there is a hfc tensor for the interaction of a proton with the unpaired spin density on each of these atoms. The total hfc tensor for the proton is the sum of these individual hfc tensors. From the crystal structure of poplar PCy the individual and total hfc tensors can be calculated. Using the angle selection technique along with the principal values of the hfc tensor the peaks in the ENDOR spectra can then be assigned to particular protons. Calculation and interpretation of the total hfc tensor is discussed in chapter 3.

#### **COMPUTER APPLICATIONS**

With the unpaired spin density in PCy delocalized over several atoms the hfc tensors for the protons in PCy can not be calculated in the straightforward manner discussed in chapter 2. In this situation the calculation of these tensors becomes more complex. Adding to the difficulty of the problem is the fact that the crystal structure for PCy does not include the coordinates for the protons. These coordinates are needed in order to extract their hfc tensors. In order to solve this problem the application of computers is necessary. The methods used to determine the nuclear coordinates of the protons and their hfc tensors along with the computer programs used in this effort are described below.

## **Crystal Structure**

The nuclear coordinates from the crystal structure of the oxidized form of PCy were obtained from the Protein Data Bank. These coordinates are listed in units of angstroms and are relative to the crystallographic axis system. This axis system is orthogonal with its origin located outside the protein structure. The crystal structure was solved by using X-ray radiation, which does not allow the nuclear coordinates for protons to be determined.

The nuclear coordinates for the protons were therefore calculated by using the program PROTIN<sup>45</sup> in conjuction with the crystal structure. This program uses idealized coordinates for the nuclei, including the protons, for all the amino acids. These coordinates are overlayed onto the protein's crystal structure and the

coordinates of the protons are calculated relative to the crystal axis system. The coordinates from PROTIN were compared to those from neutron diffraction studies of single crystals of the individual amino acids. 46,47 Comparison of geometric parameters such as bond lengths and bond angles showed good agreement. The results for the amino acids histidine and cysteine are listed in Table 1. The coordinates calculated for the protons are assumed to be accurate simulations of the true proton coordinates.

Table 1: Bond lengths and bond angles from PROTIN and neutron diffraction for histidine and cysteine

Amino Acid	Geometry	PROTIN <sup>a</sup>	Neutron <sup>a</sup> Diffraction
b Cysteine	C(1)-H(2) C(1)-H(3) C(2)-H(4)	1.067 1.068 1.045	1.077 1.076 1.104
	∠S-C(1)-H(2)	107.3	107.3
	∠H(3)-C(1)-H(2)	109.2	107.8
<sup>C</sup> Histidene	N(3)-H(10)	1.080	1.026
	N(2)-H(9)	1.060	1.070
	C(6)-C(5)	1.080	1.075
	∠C(6)-N(3)-H(10)	125.5	127.9
	∠C(5)-N(3)-H(10)	123.6	123.0

a Bond lengths are in angstroms and bond angles in degrees B Ref 46

## **Tensor Calculation**

The calculation of the total hfc tensor first involves calculating the individual hfc tensors for each component of unpaired spin density in the system. For PCy the spin density is delocalized onto the ligand atoms (His37)N, (His87)N, (Cys84)S and the copper atom.<sup>21</sup> The protons studied in this work are not bonded to amino acids

that contain unpaired spin density or are sufficiently removed from it that they have no isotropic component to their hyperfine couplings. The hfc for these protons is taken as purely dipolar and the coupling to the four sources of unpaired spin density is calculated with equation 7.

$$A_{Dip} = g \beta g_N \beta_N (3\cos^2\theta_{A}-1)/r^3$$
 (7)

Solving equation 7 for values of  $\theta_A$  of  $0^O$  and  $90^O$  yields the principle components  $A_{\parallel}$  and  $A_{\perp}$ , respectively, for the hfc tensor. The axis system for this tensor is defined such that the vector connecting the unpaired spin density with the proton is labelled the Y direction. Since the tensor is axial the directions of the X and Z axis are arbitrary and are defined so that a right handed orthogonal axis system is established.

The second step in calculating the total hfc tensor is the addition of the individual tensors. The difficulty of this process arises from the fact that the individual hfc tensors, each in its own axis system, must all be in a common axis system before they can be summed. The individual tensors must first then be rotated into the common axis system. Any axis system is suitable to be used as the common axis system. For PCy the principal axis system of the g-tensor was chosen as the common axis system. The g tensor for PCy is slightly rhombic but for this work it is assumed to be axial. The error resulting from this assumption is minimal since the difference between  $g_X$  and  $g_y$  is very small. This axis system, then, has only one unique directional component  $g_Z$ . Single crystal EPR work has placed the Z-direction of the axis system colinear with the vector between the copper atom and the sulphur atom of the methionine ligand. The X and Y directions are defined so that a right handed orthogonal system is constructed.

The values of the components of the hfc tensor after rotation into the common axis system are calculated by using equation 8.

$$A^{T}(I)_{ij} = \sum a_{ki} a_{ij} A^{T}(I)_{ki}$$
 (8)

 $A^{T}(I)_{kl}$  = hfc tensor in its principle axis system

 $A^{T}(I)_{ij}$  = hfc tensor in common axis system

 $a_{ki}$ ,  $a_{li}$  = direction cosines

$$1,2,3 = X, Y, Z$$

For the direction cosine terms the first subscript refers to the hfc system and the second to the common axis system.

With all the hfc tensors rotated into the common axis system the tensors are then summed, equation 9.

$$A^{T}_{ii} = \sum A^{T}(I_{k})_{ii} \tag{9}$$

 $A^{T}$  = total hfc tensor

 $A^{T}(I_{k}) = k^{th}$  individual tensor

The final step is to solve for the eigenvalues and eigenvectors of the total hfc tensor. This is accomplished by using the the  $IMSL^{49}$  subroutines for matrix diagonalization. The resultant eigenvalues are the principal components of the hfc tensor,  $A_X$ ,  $A_Y$ ,  $A_Z$  and the eigenvectors define the axis system of the tensor relative to the common axis. The value of the principal components along with their directions can now be compared with the angle selection ENDOR results to assign the ENDOR peaks to protons within the protein.

# **Program: TENSOR**

The program TENSOR calculates the total hfc tensor and solves for its eigenvalues and eigenvectors by following the steps described above. The program was written in Fortran 77 and run on a VAX 11/750. The matrix diagonalization was accomplished by using the IMSL<sup>49</sup> subroutine EVCRG. The IMSL subroutines WRRRN and WRCRN,<sup>49</sup> which print out the results from EVCRG, were also used. The input needed for the program is listed in Table 2 and the number of individual tensors that can be calculated is only limited by the resources of the computer.

Table 2: Input for TENSOR

$z_x, Z_y Z_z$	The coordinates of the Z axis of the common axis system relative to the crystal structure
NT	number of individual tensors to be calculated
$H_x$ , $H_y$ , $H_z$	coordinates of proton
$S_x, S_y, S_z$	coordinates of atom containing unpaired spin density
ISO	isotropic coupling for the proton
D	quantity of unpaired spin density

The last three lines of input are repeated for each atom containing unpaired electron spin density. The output of the program consists of the total hfc tensor and the tensor's eigenvalues and eigenvectors. A listing of the program is given in Appendix A.

## RESULTS AND DISCUSSION

EPR and ENDOR spectra were recorded for the blue copper protein Plastocyanin. The ENDOR measurements focused on the matrix region, the region of the spectra near the free proton resonance. The ENDOR resonances in this region are from protons that are within approximately 6 Å of the copper site and show purely dipolar hfc.<sup>50</sup> The ENDOR spectra were recorded at a series of magnetic fields within the EPR spectrum so that the angle selection technique in conjunction with the computational techniques discussed in chapter 3 could be applied. Assignment of the peaks in the ENDOR spectra to particular protons is possible by comparison of the experimental hfc values with those that were calculated. The results derived from using this technique along with consideration of the applicability of the angle selection technique to protein systems such as PCy are discussed below. The EPR spectrum was also thoroughly studied by accurately simulating the spectrum. These simulations allow the values of the terms in the spin Hamiltonian to be determined. The results from these simulations are also discussed below.

## **EXPERIMENTAL**

The EPR spectrum was recorded at X-band on a Bruker ER200D series spectrometer by using a Bruker TE<sub>102</sub> cavity. During the EPR experiment the magnetic field is modulated at 100KHz which results in the first derivative spectrum being recorded. The EPR spectrum was recorded at sample temperatures of 10±3

K. These temperatures were achieved by using an Oxford Instruments helium flow cryostat (ESR900) connected to an Oxford digital temperature controller (DTC-2).

ENDOR spectra were recorded at X-band with a Bruker ER250 Endor accessary and a Bruker ER250ENB cavity. The ENDOR coil is home built and is a modification of the design of Hurst et al.<sup>51</sup> The coil consists of 19 turns of silver wire connected to brass fittings on either end. The coil and cavity are fitted to an Oxford Instruments continuous flow helium cryostat (ESR900); spectra were recorded at sample temperatures of  $10\pm3$  K. Radiofrequency power is supplied to the coil by an ENI 3100L amplifier driven at RF frequencies generated by a Wavetek (3000-446) synthesizer. The RF power is frequency modulated, which produces a first derivative ENDOR spectra.

In the ENDOR experiments on PCy the frequency modulation (FM) of the RF power used was ±40 KHz. FM values lower than this did not reveal any better resolution within the ENDOR spectra; higher FM values resulted in line broadening and lower resolution.

In order to obtain accurate simulations of the EPR spectra the microwave frequency and magnetic field values must be known accurately. These values were measured directly by using a Bruker ER035M NMR gaussmeter and a Hewlett-Packard 5424 counter/5255 3-12 GHz converter, respectively.

Plastocyanin protein was isolated from spinach leaves using previously established procedures.<sup>60</sup> The final concentration of the protein was  $100 \mu M$ . In the deuterium substitution experiment the protein was redsuspended in an excess of D<sub>2</sub>O for 24 hours. After this period the protein was concentrated back to its original concentration.

The X-band EPR spectrum of PCy recorded at 10 K is shown in Figure 6 and the instrument parameters are listed below the spectrum. The EPR characteristics of BCP,  $g_{\parallel} > g_{\parallel}$  and a small copper  $A_{\parallel}$ , are clearly illustrated in the EPR spectrum of PCy. At X-band the slight rhombicity in the g-tensor is not detected, instead the derivative shaped portion of the spectrum appears with an effective  $g_{\parallel}$  between that of  $g_{x}$  and  $g_{y}$ . Also, the  $A_{\parallel}$  component of the copper hfc tensor is unresolved. Accurate values of the principal components of the g- and hfc tensors can not be determined from the experimental spectrum but must be obtained from computer simulations.

The EPR spectrum was simulated by using the program QPOW.<sup>52</sup> The input for the program is divided into two groups. The first group includes the experimental parameters, the microwave frequency and the magnetic field. The second group is the hamiltonian components g<sup>T</sup>, g<sub>N</sub>, A<sup>T</sup>, and the Euler angles defining the non-alimment of the tensors. Using these parameters the spin hamiltonian is solved to determine where the EPR resonances will occur. Since the samples used are frozen solutions the hamiltonian is solved for all molecular orientations to obtain the powder pattern spectrum.

The parameters in the second group are adjusted after comparison of the experimental and simulated spectra until an accurate simulation is obtained. That is, we employ an interative fit with human judgement in the feedback loop. The  $g_{\parallel}$  and  $g_{\perp}$  portions of the spectrum were expanded independently to aid in producing a more accurate simulation. The same parameters used in these simulations were also used in the simulation of the complete EPR spectrum. The simulated spectrum is shown in Figure 6 and the parameters used to simulate the spectrum are listed in Table 3.

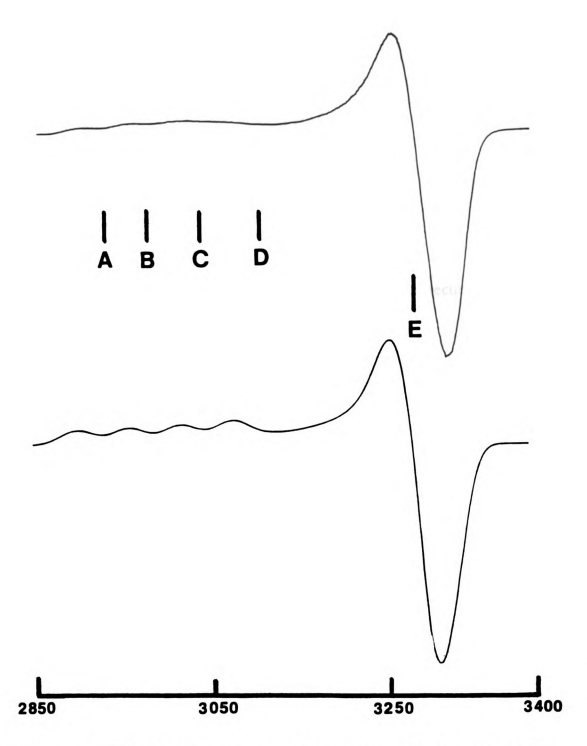


Figure 6

a) EPR spectrum of PCy. Conditions: microwave power, 2.07 mW;
12.5 KHz modulation amplitude, 0.4 Gpp; microwave frequency,
9.45543 GHz; sweep time, 200 sec. b) Simulation of (A) using
parameters in Table 1.

Table 3: Parameters for simulating the EPR spectrum of spinach PCy.<sup>a</sup>

 $g_{x} = 2.039 \pm 0.002$   $g_{y} = 2.061 \pm 0.002$   $g_{z} = 2.260 \pm 0.01$   $A_{x} = 30.0 \pm 0.5 \text{ MHz}$   $A_{y} = 30.0 \pm 0.5 \text{ MHz}$   $A_{z} = 180.0 \pm 5 \text{ MHz}$ Linewidth: X = 52.0 Y = 52.0 Z = 70.0 MHz MHz

The g- and A-tensors are colinear

Frequency =  $9.465 \, \text{GHz}$ 

Even though the experimental spectrum shows axial g-tensor characteristics a good simulation could not be obtained without using a rhombic g-tensor. The g<sub>1</sub> region of the spectrum was also very sensitive to variation in  $g_X$  and  $g_Y$ . Changes of less than 1% in the values of  $g_X$  and  $g_Y$  caused significant distortion in the lineshape. The values of g<sub>x</sub> and g<sub>y</sub> reported in Table 1 are very close to those obtained from Qband EPR spectra of PCy where  $g_x = 2.042$  and  $g_v = 2.059$ . The value of  $g_{\parallel}$  has a slightly larger error due to the significant amount of g- and A-strain present in this portion of the spectrum.<sup>53</sup> The value we determined for  $g_{\parallel}$  is slightly larger than the previouly measured value of 2.23 for PCy at 25 K.54 The difference is probably a result of the fact that the authors of the earlier study were unable to measure accurately the microwave frequency or magnetic field.

The hfc tensor components were similar to the g values in that the error in  $A_{\perp}$  is approximately 1.5% where the error in  $A_{\parallel}$  is larger at about 3%. The larger error in A<sub>1</sub> is again the result of g- and A-strain. Our value for A<sub>1</sub> of 180 MHz is very similar to the previously reported value of 189 MHz.<sup>54</sup> For A<sub>1</sub> previous work

<sup>&</sup>lt;sup>a</sup>The error reported for these values are determined by visual inspection of the simulations

could only estimate its magnitude to be less than 51 MHz.  $^{14}$  The present work shows that  $A_1$  is 30 MHz.

On the EPR spectra in Figure 6 are marked the positions (A-E) where the ENDOR spectra were recorded. ENDOR spectra were recorded over the entire range from  $g_{\parallel}$  to  $g_{\parallel}$  so that the angle selection technique could be applied.

#### **ENDOR**

The ENDOR spectra of PCy recorded at positions A-E on the EPR spectrum are shown in Figures 7 and 8. From these spectra seven sets of proton ENDOR resonances were observed. The magnitude of the hfc constant for each set of peaks along with their lineshape types are listed in Table 4. Assignment of the ENDOR resonances to protons within the protein was based on two criteria, comparison of the experimental ENDOR couplings with the calculated hfc tensors and the value of  $\theta_P$  for the tensor components.

Table 4: Pairs of resonances from the ENDOR spectra of spinach PCy.

Peak pair	hfc constant(MHz) <sup>a</sup>	Lineshape	
a,a´	5.13	absorptive	
b,b′	3.19	absorptive	
c,c′	2.30	absorptive	
c,c′ d,d′	2.14	absorptive	
e,e´	1.61	derivative	
e,e´ f,f´	1.15	derivative	
g,g´	0.92	rhombic	

<sup>&</sup>lt;sup>a</sup>The error in these values is discussed in the text

The hfc tensors for these protons were determined by using the coordinates obtained by the procedure discussed in chapter 3. These coordinates, though, are based on the crystal structure of plastocyanin from poplar. The spinach and poplar

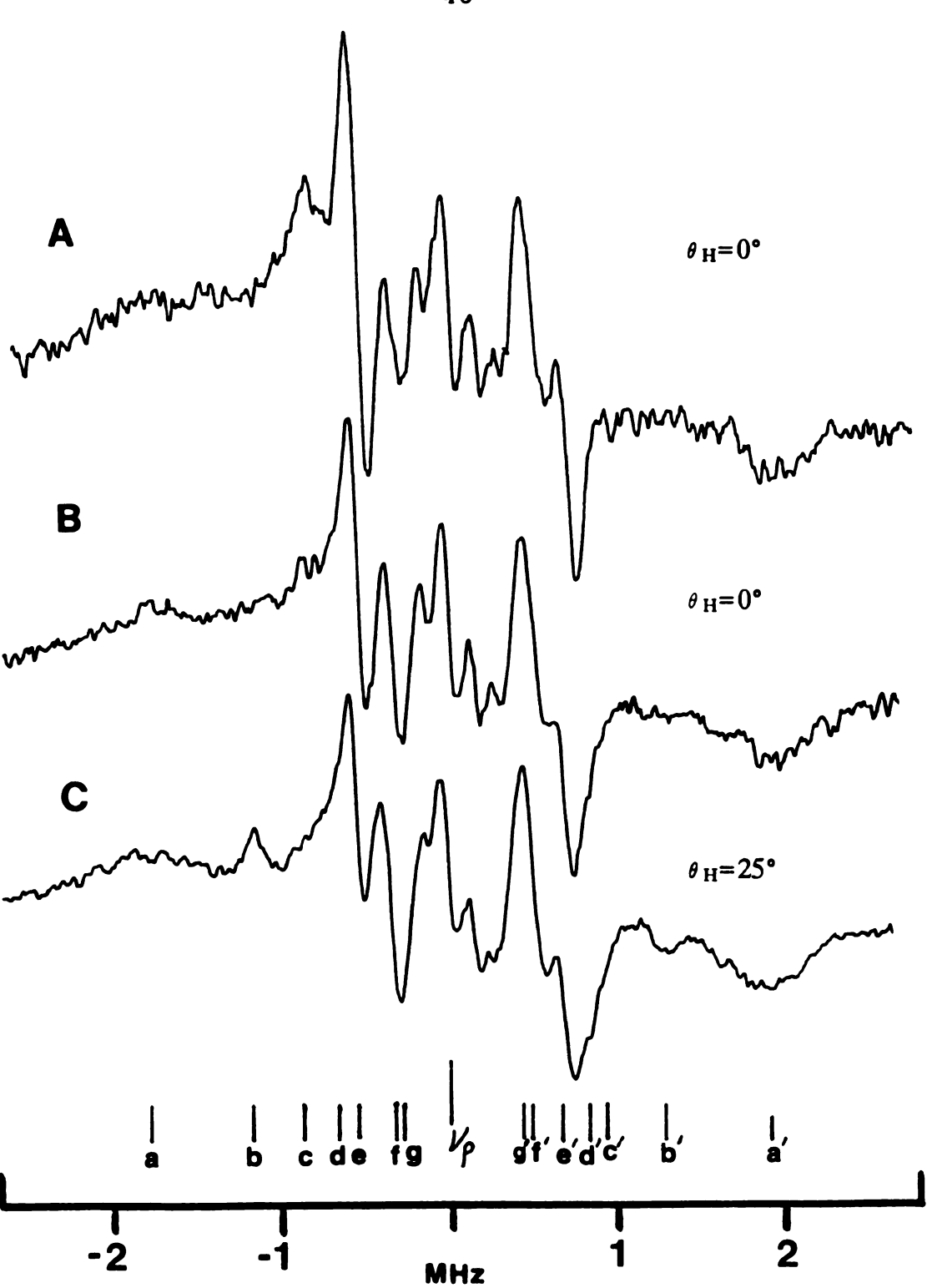


Figure 7 ENDOR spectra of PCy for the positions marked A,B, and C in Figure 6. Conditions: microwave power, 20.7 mW; microwave frequency, 9.4355 GHz; RF power, 90 W; RF modulation frequency, 40 KHz; sweep time 200 sec.

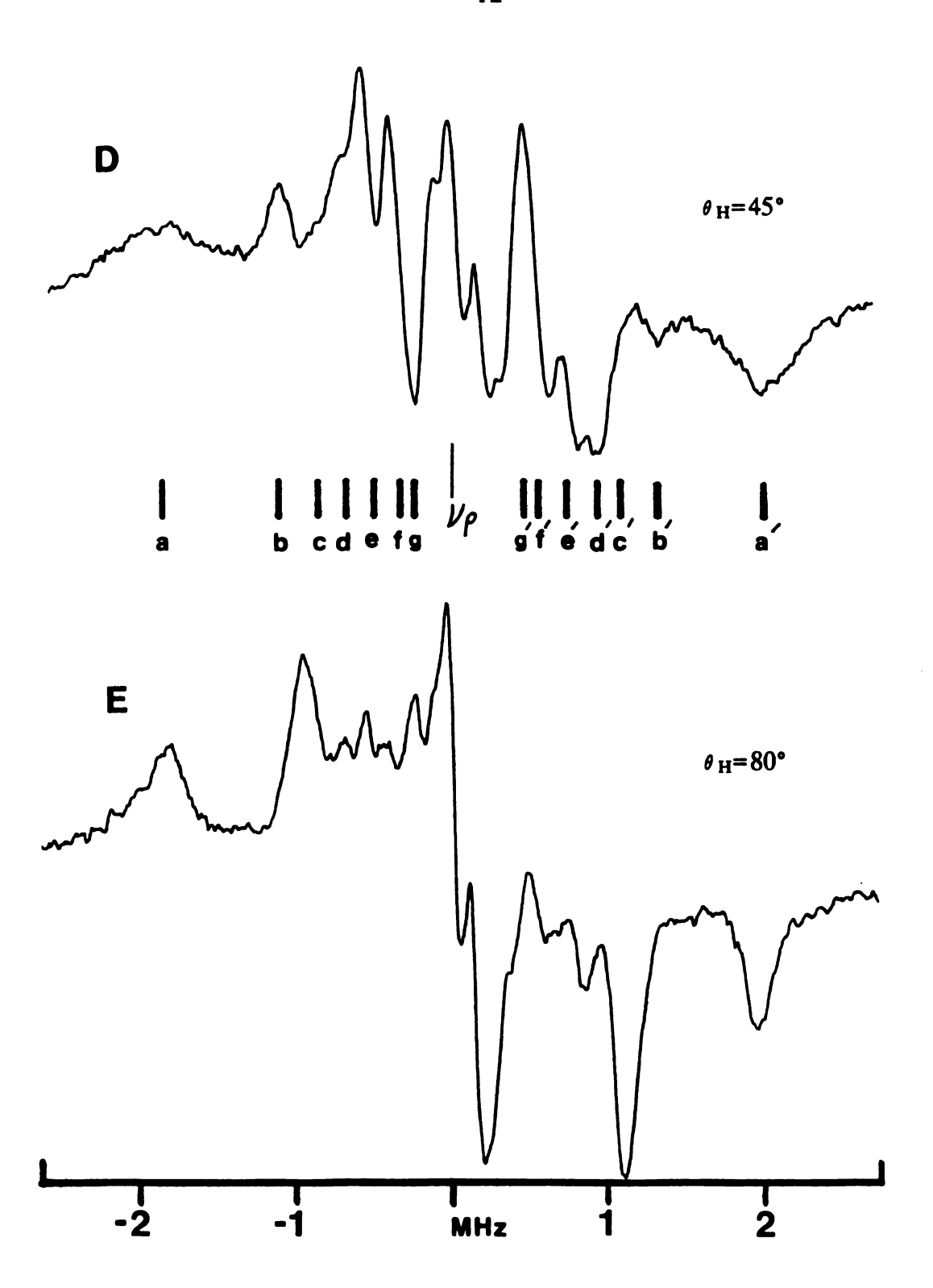


Figure 8 ENDOR spectra of PCy for the positions marked D and E in Figure 6. Conditions: same as in Figure 7.

forms of the protein both have 99 amino acids and only differ in amino acid type at 22 locations. The majority of these amino acid substitutions involve conservative changes and surface residues. These types of changes in amino acids should not cause significant differences in the tertiary stuctures of the two proteins. NMR experiments, in particular NOE techniques, have been used to determine any structural differences between spinach plastocyanin and the crystal structure of poplar plastocyanin. A qualitative comparison of the NOE data obtained for spinach PCy and inter-proton distances calculated from the crystal structure showed no inconsistencies. The NOE data included backbone-backbone short- and long range interactions as well as sidechain-sidechain interactions. From this large set of data it was concluded that the structure of poplar plastocyanin is conserved in spinach even with the amino acid substitutions. The proton coordinates calculated by using the poplar plastocyanin crystal structure are thus assumed to be the same or nearly the same for PCy.

Of all the protons in PCy there are 28 that are near enough to the copper site to give ENDOR peaks that are resolvable. The criterion used to select these protons was that they have at least one component of their hfc tensor equal to 1 MHz or greater. This is the minimum coupling that is resolvable within the ENDOR spectra. The 28 protons are located on eight amino acids including the four ligand amino acids. These eight amino acids are conserved between the poplar and spinach forms of the protein.

Since the exact distribution of the unpaired spin electron density is not known the hfc tensors were calculated by using a series of different distributions. As a starting point, the calculated distribution by Penfield and co-workers of Cu 45%, S 35%, N 10% and N 10% was used.<sup>21</sup> An ENDOR study of a large number of pseudoplanar copper complexes with nitrogen and oxygen ligands showed that the spin density on the nitrogen was between 6% and 10%.<sup>20</sup> The different

distributions we used in calculating the hfc tensors had low or no spin density on the nitrogen ligands and varied the majority of the spin density between the copper and sulphur atoms. The different spin density distributions (SDD) groups are listed in Table 5.

Table 5: Spin density distributions used in calculating hfc tensors.

SDD group <sup>a</sup>	%Cu	%S	%N	%N
1	55	35	5	5
2	65	35	0	0
3	50	50	0	0
4	70	30	0	0
5	45	35	10	10

<sup>&</sup>lt;sup>a</sup>SDD = spin density distribution

Along with calculating the hfc tensor for the 28 protons the orientation of the tensor relative to the g-tensor axis system is also determined. Since the g-tensor is treated as axial in this work the only unique axis is  $g_{\parallel}$ . The only orientational information then that is relavent is the angle  $\theta_B$ , which is the angle between the direction of the tensor component and the direction of  $g_{\parallel}$ . As the value of  $\theta_H$ , the angle between the applied magnetic field and  $g_{\parallel}$ , increases, and the applied magnetic field becomes closer aligned along the direction of the hfc tensor component, the intensity of the ENDOR peaks will increase. The intensity of the peaks then will be a maximum when  $\theta_P = \theta_H$ . The value of  $\theta_P$  is then used to find that proton whose hfc tensor would best match the intensity changes seen in the experimental spectra.

The error in the calculated hfc tensor components was determined from the error reported for nonbonded atom contact in the crystal structure. This error was estimated to be 0.5 Å. 1 Coordinates were then determined for the atoms containing

unpaired spin density such that the distances from these atoms to a proton were equal to the crystallographic distance  $\pm 0.25$  Å. The hfc tensor was then calculated by using the longest distances and again using the shortest distances. These two sets of data repesent the maximum and minimum results for the calculations, while the results from using the crystallographic coordinates were generally half way between the two extrema. The spread in the results was considered to be the error for these calculations and was found to be 20%. This calculation was carried out for several protons, both close and far from the unpaired spin density, and the error was always found to be about 20%. The variation in  $\theta_P$  is much less sensitive to the change in distances between atoms discussed above. The value of  $\theta_P$  changes by only a few degrees between the maximum and minimum result data sets.

## **ASSIGNMENTS**

Reliable assignment of the ENDOR peaks to one particular proton, or in some cases two protons with nearly identical characteristics, is possible for four of the pairs of ENDOR resonances. In the other three cases, due to discrepancies in both hfc values and  $\theta_P$  the assignment of the ENDOR resonances was not possible. These assignments along with the complete hfc tensor for the protons are listed in Table 6.

## Peaks a,a'

The peak pair a,a' have an absorption lineshape and a coupling of  $5.13\pm1$  MHz. The intensity of these peaks shows an increase up through  $\theta_H = 45^{\circ}$  and nearly the same intensity at  $\theta_H = 80^{\circ}$ . This intensity change indicates that  $\theta_P$  is located between these two values of  $\theta_H$ . There are two protons that match these

characteristics, the amide proton on asparagine 38 (A38H) and a proton on the  $\beta$ -carbon of histidine 87 (H87HB1). For H87HB1 the hfc values range from 4.23-5.33 MHz while  $\theta_P$  varies from  $66^{\circ}$ - $68^{\circ}$  for the five spin density distributions. The hfc values for A38H vary from 4.59-4.98 for SDD groups 1,2,4,5 while the value for SDD group 3 is much larger at 6.22. The angle  $\theta_P$  again varied little,  $59^{\circ}$ - $62^{\circ}$ . With the small difference in hfc and  $\theta_P$  values assignment of the peaks to one proton or the other is not possible.

## Peaks b.b'

This pair of peaks, with a coupling of  $3.19\pm0.60$  MHz, also has an absorptive lineshape. These peaks first appear when  $\theta_H = 25^{\circ}$  and the intensity is increasing even when  $\theta_H = 80^{\circ}$  indicating that  $\theta_P$  must be at or near 90°. Five protons have values for the absorptive components of their hfc tensors that are near 3.20 MHz. Only the proton on the  $\beta$ -carbon of histidine 37 (H37HB2) has the correct value of  $\theta_P$  with 90°. For the other protons  $\theta_P$  ranged from 67° down to 20°. The value of this tensor component for H37HB2 varies from 3.07 to 3.75 MHz for the five SDD groups whereas the value of  $\theta_P$  varies by only a few degrees.

## Peaks d.d'

These peaks, with an absorptive lineshape and a coupling of  $2.14\pm0.36$  MHz, are present as shoulders on peaks e,e'. The peaks are first present when  $\theta_H=25^{\circ}$  and increase in intensity until  $\theta_H=45^{\circ}$ . When  $\theta_H=80^{\circ}$  the intensity of these peaks has decreased. The value of  $\theta_P$  should then be in the range of  $45^{\circ}-80^{\circ}$ . Once again a series of protons, five, have the correct hfc values for the ENDOR coupling. Three of these protons have  $\theta_P$  values that are too small,  $18^{\circ}-37^{\circ}$ , while one is too

large,  $\theta_P = 80^{\circ}$ . The proton that meets both criteria is the second proton on the  $\beta$ -carbon of histidine 87 (H87HB2). For SDD groups 1,2,4 and 5 the hfc values range from 1.77-1.83 MHz and  $\theta_P$  varies from 63°-67°. For SDD group 3 the hfc value is too low at 1.65 MHz.

# Peaks f,f'

Peak pair f,f' are derivative shaped peaks with a coupling of  $1.15\pm0.20$  MHz. The intensity changes of these two peaks is very much like that of the pair d,d'. The intensity of the peaks is increasing when  $\theta_H=45^{\circ}$  but the peaks are very small or not present at all at  $\theta_H=80^{\circ}$ . Again this will place  $\theta_P$  within this range. Two protons with nearly identical characteristics are assigned to these peaks. The proton on the  $\beta$ -carbon of methionine 92 (M92HB2) has hfc values that range from 0.94-1.01 MHz and a  $\theta_P$  that ranges from 37°-40° for SDD groups 1-4. The hfc value for SDD group 5 is lower at 0.88 MHz.

The second proton is the terminal -CH<sub>3</sub> group of the methionine 92 side chain. At a sample temperature for these spectra of 10 K, the methyl group is assumed to be rotating freely. The three protons are then magnetically equivalent and the methyl group is represented by a single proton at the average position of the three protons. EPR studies of organic radicals such as the chloroacetylalanine<sup>56</sup> and 4-methyl-2,6-ditertbutylphenol<sup>57</sup> free radicals have shown that methyl groups can be freely rotating even at temperatues of 4.2 K. The methyl groups of bis(acetylacetonate) copper (II) in frozen solutions have also been shown to be freely rotating at 25 K as determined by ENDOR.<sup>44</sup> A study of the PCy crystal structure also shows that the -CH<sub>3</sub> group is located in a pocket where there is no protein structure to hinder its rotating.

The hfc and  $\theta_P$  values for M92CH3 are very similar across all five SDD groups. The hfc values range from 1.22-1.34 MHz while  $\theta_P$  only changes slightly from 57°-59°. As in the case for peaks a,a' the hfc and  $\theta_P$  values for the two protons are so similar that assignment of peaks f,f' to just one proton is not possible.

# Peaks c,c'; e,e'; g,g'

For each of these sets of peaks a reasonable assignment to one or more of the protons in PCy was not possible. It was possible to assign one or more protons to each set of peaks on the basis of hfc values alone but in each case the values of  $\theta_P$  were significantly in error. Possible explanations for the inability to assign these peaks are discussed later in this chapter.

Table 6: Protons assigned to the ENDOR spectra and their complete hfc tensors.

Peaks	Proton	A <sub>X</sub>	Ay	Az	
a.a´	H87HB1	-1.9	-2.9	5.1	
a,a ´ a,a ´	A38H	-2.1	-2.6	4.7	
b,b′	<b>H37HB2</b>	-1.3	-2.1	3.5	
ďď.	H87HB2	-0.8	-1.0	1.8	
d,d′ f,f′	M92HB2	-0.8	-1.0	1.8	
f,f′	M92CH3	-1.1	-1.3	2.4	
-					

## **DEUTERATION**

In conjunction with the calculated hfc tensors another method that would assist in the assignment of the ENDOR spectra would be deuterium substitution. If a deuterium could be substituted for a proton whose peaks were present in the

ENDOR spectra, those peaks would disappear. There are several exchangeable protons near the copper site that could possibly be substituted.

The ENDOR spectra for the deuterated sample of PCy were taken at magnetic fields similar to those for the protonated sample. These spectra showed no difference when compared with those taken for the protonated sample. All seven sets of peaks were present and they showed the same hfc constants. The intensity changes as a function of magnetic field of the peaks seen in the spectra of the protonated sample were reproduced in the spectra of the deuterated sample. These results are consistent for the four sets of peaks in which assignments were made since all these protons are covalently bonded and are not expected to exchange. Of the 28 that are near the copper site only five, all backbone amide protons, are expected to be exchangable. NMR studies of PCy have shown that four of these five protons are non-exchangeable even after dissolving the protein in a D<sub>2</sub>O buffer for 24 nours.<sup>33</sup> The only proton that did exchange was the amide proton on histidine 87. The deuteration experiments are thus consistent with the assignments made above for the peaks labelled aa', bb', dd', and ff'. Moreover, the deuterium work allows us to conclude that the three sets of unassigned peaks are not derived from the amide proton of histidine 87.

## SPIN DENSITY DISTRIBUTION

The different SDD groups used to calculate the hfc tensors are listed in Table 5. It was expected that one of these groups would consistently prevail over the other groups in giving the correct hfc constants and  $\theta_P$  values and thus the correct SDD could be determined. This approach was used in the study of the unpaired spin distribution in benzoquinone and the tyrosine radical in ribonucleotide reductase. The distribution was changed until the calculated hfc

tensors for each proton matched the experimental values determined using ENDOR. By using an iterative process the distribution of the unpaired spin was determined.

The hfc tensors for H87HB1, H37HB2, M92HB2 and M92CH3 showed little difference when the different SDD groups were used in their calculation. The calculated tensors in each case gave reasonable results for all five SDD groups. The only exceptions were the protons A38H and H87HB2. For H87HB2 the hfc tensor component with SDD group 3 was 1.65 MHz, which is significantly lower than the values for the other four SDD groups and below the range of 1.78-2.50 MHz for this hfc constant. Similar results were seen for A38H except that in this case the tensor component was much larger, 6.22 MHz, which is outside the range of 4.13-6.13 MHz for this set of peaks. There also were no situations where a proton assignment could be made only by using the hfc tensor calculated using SDD group 3. The SDD group 3 only gave viable results in those cases where the calculated tensor was insensitive to the spin density distribution. From these results it appears that the distribution with the unpaired spin density split equally between the copper and sulphur atoms is incorrect. The best results are obtained with a greater portion of the unpaired spin density on the copper atom versus the sulphur and when the distribution on the sulphur atom is no more than 35%. Any higher resolution of this unpaired spin density is not possible from these results.

## DISCUSSION

The technique of angle selection ENDOR has proved successful in assigning many of the resonances in the ENDOR spectra of PCy. The complete hfc tensors for the protons that have been assigned to the ENDOR spectra are listed in Table 6. In each case, though, only one component of the hfc tensor could be identified.

There are several possible reasons why the other components were not detected. The ENDOR resonance for each hfc tensor component will have its own properties with respect to relaxation. That is, the transitions between nuclear spin states giving rise to the ENDOR resonances (Figure 4) have different relaxation rates. If this relaxation is fast on the ENDOR time scale then the ENDOR resonances will be broadeded out and, in extreme cases, not detectable. The intensity of ENDOR peaks is dependent on several factors including microwave power, RF power and temperature. In this experiment these parameters were varied over a modest range about the optimum conditions without resolving any new resonances.

A second explanation is the high density of resonances within this region of the spectrum. The four protons that have been assigned have ten resonances, of different lineshapes, with couplings of less that 3 MHz (Table 6). In many cases tensor components from two different hfc tensors are nearly the same. If one of the resonances is present but is severely broadened, as discussed above, and has a low intensity relative to a second resonance, with a large intensity, the first resonance may not be detected. In this system the reason that some of the hfc tensor components are not detected is most likely a combination of both effects.

For the three ENDOR resonances that could not be assigned to any protons the most likely reason is small structural differences between poplar and spinach PCy. While the NMR NOE studies indicate that the overall structure of the two proteins are very similar, these experiments do not have the resolution to detect small differences in structure. For a long side chain amino acid such as methionine or histidine a slight change in several bond angles could cause a moderate change in the position of a hydrogen bonded to the sidechain. The discussion on the errors in the calculated hfc tensors showed that even the relatively small shifts in atomic position of 0.5 Å can cause a significant change in the tensor components. These results then indicate that while the magnitude may be small there is probably some

structural differences between poplar and spinach PCy. Since the exact unpaired spin density distribution could not be determined it was not possible to determine which protons had moved or the direction and amount of the movement.

Several different BCP, including two species of PCy have previously been studied by ENDOR. <sup>38,39</sup> In these experiments ENDOR was used to detect and study the nitrogen ligands to the copper and to study the proton resonance with a coupling of 27 MHz. This large coupling was proposed to come from the methylene group of the amino acid cysteine 84, which also contains the sulphur ligand. This coupling is large as a result of the significant amount of unpaired spin density on the sulphur atom, which gives these two protons a large isotropic component to their hfc constant. This same resonance was also seen in the present work (spectrum not shown). The ENDOR spectra for PCy from the species bean and poplar were found to be very similar in all aspects. The spectra from these experiments, though, were very low in resolution and showed only one set of proton resonances near the free proton resonance. No attempt was made to acheive higher resolution spectra or to study intensity changes of the resonances. The present work is the first attempt to detect and assign the matrix region couplings in the ENDOR spectra of a PCy.

It has been shown here that structural and electronic information can be obtained for biological species by using the angle selection ENDOR technique. It is also important to note that the information was obtained from frozen solution spectra and not from single crystals. Since single crystals have not been produced for many of the biological species under study there are many systems where this technique could prove very useful. In this work two sets of structural data were determined. First, for those protons that could be assigned to the ENDOR spectra their positions within the protein are the same as the corresponding proton in poplar PCy. Second, this work has also shown that there are some structural differences, although probably small, between the poplar and spinach forms of PCy.

With the use of several other techniques, including molecular biology and biosynthesis, it is expected that assignments made in the ENDOR spectra can be made less equivocal. That is, for those ENDOR resonances where two protons were assigned or for those resonances in which no assignments could be made, these methods will help in determining the exact assignment. These approaches are considered briefly in the following chapter.

## **FUTURE WORK**

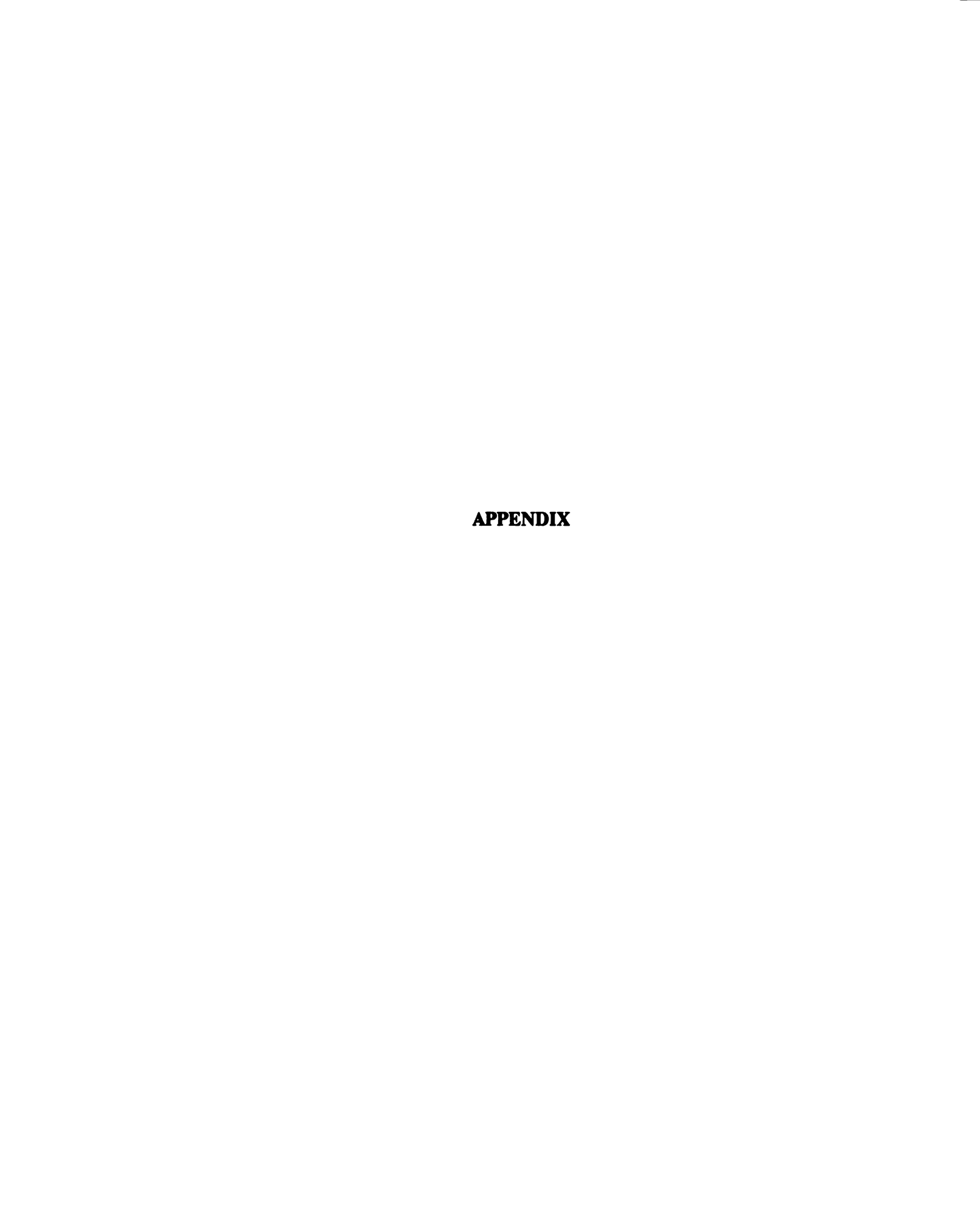
The assignments to the ENDOR spectrum discussed in the previous section were based on solid theoretical approaches. Since no substitution occurs in the deuterium exchange experiment it was not possible to confirm these results. Our future efforts are aimed at securing a technique in which deuterium substitution can be accomplished and the exact site of substitution can be controlled. Substitution of a proton that already has been assigned will be the most useful in confirming the results obtained in this work. One possible approach for achieving the goal of selective deuteration is the use of amino acid auxotrophs.

Auxotrophs are mutants of a species that require the addition of a certain amino acid in the growth medium for the species to grow. Unfortunately, there are few reports of plant amino acid auxotrophs.<sup>61</sup> However, there are auxotrophs for photosynthetic cyanobacteria, which also contain the protein plastocyanin. The cyanobacteria strain Anabaena variabilis has a methionine auxotroph.<sup>62</sup> Peaks f,f' in the ENDOR spectrum of PCy have been assigned to either a proton on the  $\beta$ -carbon or the protons of the terminal methyl group of methionine 92. Use of this mutant with perdeuterated methionine and methionine selectively deuterated at the positions discussed above would allow exact assignment of these peaks in the ENDOR spectrum. The procedure can be followed for other auxotrophs to confirm or determine other assignments in the ENDOR spectrum.

Upon confirmation of the proton assignments ENDOR will be used to study PCy when it is bound to its redox partner cytochrome f. There is currently some disagreement as to the binding site of cytochrome f on PCy.<sup>63,64</sup> The two proposed

sites are the acid patch consisting of amino acids 42-45 on the "east" side of the protein and histidine 87 on the "north" side of the protein. If binding was to occur at the acid patch, which is approimately 12 Å from the copper site, little or no structural changes would be expected at the copper site. However, if the binding occurs at histidine 87 significant structural modifications may occur. ENDOR will be used to study the structural difference, if any, that occur near the copper site in PCy after binding to cytochrome f.

Efforts are also underway to carry out site-directed mutagenesis on PCy. One proposed modification is to substitute a cysteine for one of the non-cysteine ligands to the copper. The purpose of this experiment is to determine if a blue copper protein with two cysteine ligands mimics the Cu<sub>A</sub> in cytochrome oxidase. ENDOR, then, will be used both to determine if this substitution causes any structural changes and, more importantly, to acertain whether a second cysteine ligand causes any change in the distribution of the unpaired spin density.



## **APPENDIX A**

# **Program Listing for TENSOR.FOR**

```
00000000000
       This program will calculate a theoretical dipolar hyperfine coupling tensor, in
       any axis system. If there are several nuclei interacting with the unpaired spin
       density, the tensors will be rotated into a common axis system and then
       added. The total tensor will then be diagonalized and the direction cosines
       from the common axis system and the axis system that diagonalized the
       tensor.
             Matthew Espe
             Babcock research group
             Dept of Chemistry
             Michigan State University
REALHC(3), SD(3), GCR(3,3), HCR(3), LENA(3), D, AS(3,3), LVC(3), T(3,3), HFC(3,3), LENG(3), AC(3,3), R(3,3), SDR(3), EGVL(3), A(3,3), ISO, LPC, EGVC(3,3), MC(361), PC(361), MF, TH, STH, CTH, VN, ANG, AF, H(3),
       LH(3), LMC
       CHÀŔACTER*8 INPUT, OUTPUT
       CHARACTER*1 F.G
       INTEGER LJ,K,N,NA,B,LDA,LDEVEC,ITRING,NCA,NRA
       COMPLEX EVAL(3), EVEC(3,3)
       DATA AS,T,HFC,A,LVC/9*0.0,9*0.0,9*0.0,9*0.0,3*0.0/
C
       PRINT*, THIS IS THE PROGRAM ROTATE. IN ORDER TO USE '
       PRINT*, 'THE PROGRAM THE USER MUST HAVE'
       PRINT*,'ALREADY SET UP AN INPUT FILE WITH THE CORRECT
       SPECIFICATIONS.
       PRINT*,'PLEASE SEE THE DOCUMENTATION FOR HELP ON
       USING THE PROGRAM.'
CCC
       DATA INPUT FOR EVCRG SUBROUTINE
       N=3
       LDA = 3
      LDEVEC=3
C
       ENTERING NAME OF INPUT AND OUTPUT FILES
2000 WRITE(6,1)
```

```
FORMAT(/,/,1X,'ENTER NAME OF INPUT FILE-UP TO 8 LETTERS',/)
1
      READ(5,2) INPUT
      FORMAT(A8)
2
       WRITE(6,3)
      FORMAT(/,1X,'ENTER NAME OF OUTPUT FILE-UP TO 8 LETTERS',/)
3
      READ(5,4) OUTPUT
4
      FORMAT(A8)
      CALL UMACH(-1,9)
      CALL UMACH(-2,12)
      OPEN(UNIT=9,FILE=INPUT,STATUS='OLD')
      OPEN(UNIT=12, FILE=OUTPUT, STATUS='NEW')
C
Č
      READ IN DATA
      READ(9,7) (R(3,I),I=1,3)
      READ(9,6) NA
6
      FORMAT(I3)
      READ(9,7) (HC(I),I=1,3)
      FORMAT(3F8.4)
CCCCC
      CALCULATE G-AXIS SYSTEM
          DETERMINE G-X AXIS
      R(1,1) = 1.0
      R(1.2) = 0.0
      R(1,3) = -R(3,1)/R(3,3)
          DETERMINE G-Y AXIS
      R(2,1) = R(3,2) * R(1,3) - R(1,2) * R(3,3)
      R(2,2)=R(1,1)*R(3,3)-R(3,1)*R(1,3)
      R(2,3) = R(3,1)*R(1,2)-R(1,1)*R(3,2)
C
          LENGTH OF G-AXIS VECTORS
      LENG(1) = SQRT(R(1,1)^{**}2 + R(1,2)^{**}2 + R(1,3)^{**}2)
LENG(2) = SQRT(R(2,1)^{**}2 + R(2,2)^{**}2 + R(2,3)^{**}2)
      LENG(3) = SQRT(R(3,1)^{**2} + R(3,2)^{**2} + R(3,3)^{**2})
            DO 100 J = 1.3
               DO 100 I = 1.3
                 R(J,I) = R(J,I)/LENG(J)
100
            CONTINUE
C
      ROTATE G AXIS SYSTEM SO THAT IT IS THE ABSOLUTE AXIS
      SYSTEM.
C
      THE COORDINATES FOR THE HYDROGEN ARE ROTATED IN
      THE NEW G AXIS SYSTEM.
C
      DO 120 I = 1.3
        DO 120 J = 1.3
            HCR(I) = HCR(I) + R(I,J) * HC(J)
            DO 120 K = 1.3
               GCR(I,J) = GCR(I,J) + R(J,K) * R(I,K)
120
      CONTINUE
```

```
WRITE(10,3000) GCR(1,1),GCR(1,2),GCR(1,3)
WRITE(10,3000) GCR(2,1),GCR(2,2),GCR(2,3)
      WRITE(10,3000) GCR(3,1),GCR(3,2),GCR(3,3)
3000 FORMAT(3F8.4,/)
Č
      MAIN LOOP TO CALCULATE A-TENSOR AFTER ROTATION
      DO 1000 B = 1,NA
             READ(9,10) (SD(I),I=1,3)
             FORMAT(3F8.4)
10
             READ(9,11) ISO
11
             FORMAT(F7.3)
             READ(9.15) D
15
             FORMAT(F6.3)
CCCC
      THIS SECTION DETERMINES THE x,y, AND z COORDINATES OF
      THE X.Y. AND Z AXIS OF THE HYPERFINE TENSOR
      DO 140 I = 1.3
        DO 140 J = 1.3
             SDR(I) = SDR(I) + R(I,J)*SD(J)
140
      CONTINUE
      DO 160 I = 1.3
        AC(2,I) = HCR(I)-SDR(I)
160
      CONTINUE
CCC
      DETERMINATION OF Z AXIS
      AC(3,1) = 0.0
      AC(3,2) = -AC(2,3)/AC(2,2)
      AC(3,3) = 1.0
C
Č
      DETERMINATION OF X AXIS
      AC(1,1) = AC(2,2)*AC(3,3)-AC(2,3)*AC(3,2)

AC(1,2) = AC(2,3)*AC(3,1)-AC(2,1)*AC(3,3)
      AC(1,3) = AC(2,1)*AC(3,2)-AC(3,1)*AC(2,2)
CCC
      CONVERSION TO UNIT VECTORS
      LENA(1) = SQRT(AC(1,1)^{**2} + AC(1,2)^{**2} + AC(1,3)^{**2})
      LENA(2) = SQRT(AC(2,1)**2 + AC(2,2)**2 + AC(2,3)**2
      LENA(3) = SQRT(AC(3,1)^{**2} + AC(3,2)^{**2} + AC(3,3)^{**2})
             DO 180 I = 1.3
               DO 180 J = 1.3
                   AC(I,J) = AC(I,J)/LENA(I)
180
             CONTINUE
C
      CALCULATION OF A TENSOR DIAGANOL COMPONENTS
      HFC(1,1) = (-78.4*D)/LENA(2)**3
      HFC(2.2) = (78.4*2.0*D)/LENA(2)**3
      HFC(3,3) = HFC(1,1)
```

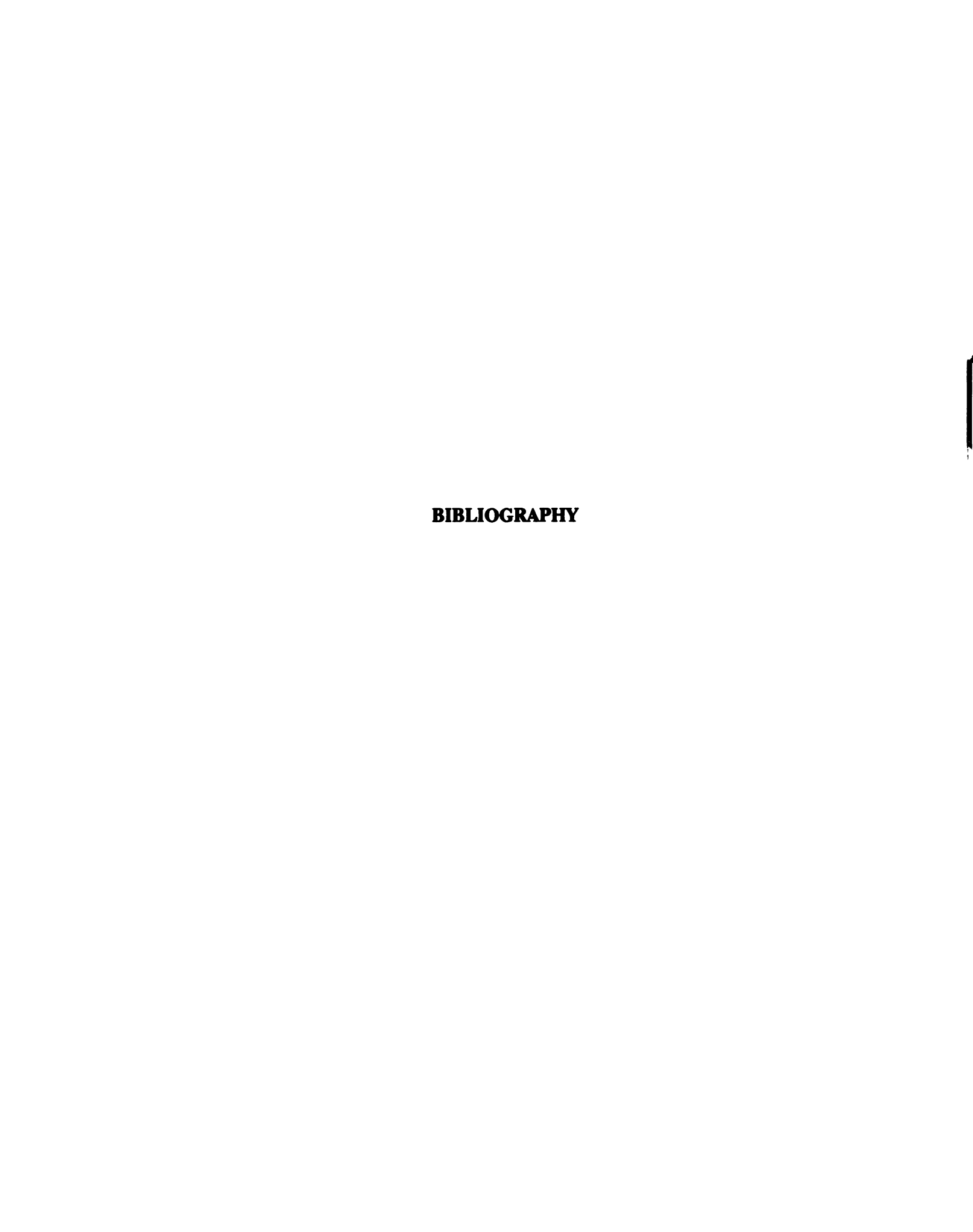
```
C C C 200
C C C C C
      CALCULATION OF DIRECTIONAL COSINES
      CONTINUE
      ROTATION OF A-TENSOR INTO CRYSTAL G-AXIS SYSTEM
       AND ADDITION OF THE A-TENSORS
      DO 240 I = 1.3
      DO 240 J = 1.3
                  DO 220 K = 1.3
      T(I,J) = AC(k,i)*AC(k,j)*HFC(k,k)
      AS(I,J) = AS(I,J) + T(I,J)
220
      CONTINUE
      A(I,J) = A(I,J) + AS(I,J)
240
      CONTINUE
CCC
      PRINTING OUT THE RESULTS
      WRITE(10.20) B
     FORMAT(1X,'COMPONENTS OF A-AXIS AND DIRECTION COSINES
20
           FOR ATOM', I2,/)
      WRITE(10,25) (AC(1,I),I = 1,3)
      FORMAT(1X,'X AXIS IN A-TENSOR SYSTEM',3(1X,F11.7))
25
      WRITE(10,30) (AC(2,I),I = 1,3)
      FORMAT(1X,'Y AXIS IN A-TENSOR SYSTEM',3(1X,F11.7))
30
      WRITE(10,35) (AC(3,I),I=1,3)
35
     FORMAT(1X,'Z AXIS IN A-TENSOR SYSTEM',3(1X,F11.7))
C
Č
     PRINTING OUT A TENSOR
C
      WRITE(10,36)
     FORMAT(/,10X,'HYPERFINE COUPLING TENSOR',/)
36
     DO 260 I = 1.3
        WRITE(10,37) (HFC(I,J),J = 1,3)
       FORMAT(1X,3(F8.5,3X))
37
260
     CONTINUE
CCCC
     PRINT OUT DIRECTION COSINES
     COMPONENTS OF A MATRIX AFTER ROTATION
\tilde{\mathbf{C}}
      WRITE(10,46)
     FORMAT(/,1X,'COMPONENTS OF A TENSOR AFTER ROTATION',/)
46
     DO 320 I = 1.3
        WRITE(10,47) (AS(I,J),J = 1,3)
        FORMAT(1X,3(F8.5,3X))
47
320
     CONTINUE
     DO 360 I = 1.3
        SDR(I) = 0.0
        DO 360 J = 1.3
           AS(I,J) = 0.0
360
     CONTINUE
C
```

```
CC
           END OF MAIN LOOP
1000 CONTINUE
CCCCCCCCC
     EVCRG IS AN IMSL LIBRARY SUBROUTINE WHICH CACULATES
     THE EIGENVALUES AND EIGENVECTORS OF A MATRIX. THE
     SUBROUTINES UMACH AND WRCRN ARE ALSO IMSL ROUTINES
     THAT CONTROL THE OUTPUT OF THE DATA FROM THE EVCRG
     ROUTINE.
                    *************************************
     CALL EVCRG(N,A,LDA,EVAL,EVEC,LDEVEC)
\mathbf{C}
     PRINTING OUT RESULTS
     call WRRRN('TOTAL A-TENSOR',3,3,A,LDA,0)
     CALL WRCRN('EIGENVALUE',1,3,EVAL,1,0)
     CALL WRCRN('EIGENVECTOR', 3, 3, EVEC, 3, 0)
C
     DO 1200 I = 1.3
       EGVL(I)=REAL(EVAL(I))
       DO 1200 J = 1.3
           EGVC(I,J) = REAL(EVEC(I,J))
1200 CONTINUE
     LVC(1) = SQRT(EGVC(1,1)**2 + EGVC(2,1)**2 + EGVC(3,1)**2)
     LVC(2) = SQRT(EGVC(1,2)**2 + EGVC(2,2)**2 + EGVC(3,2)**2
     LVC(3) = SQRT(EGVC(1,3)**2 + EGVC(2,3)**2 + EGVC(3,3)**2)
     DO 1400 I=1.3
           DO 1400 J = 1.3
            EGVC(J,I) = EGVC(J,I)/LVC(I)
1400 CONTINUE
C
Č
     CALCULATE ENDOR FREQUENCIES
Č
      WRITE(6,2005)
     FORMAT(8X,'DO YOU WISH TO CACULATE ENDOR
2005
     FREQUENCIES [Y/N]?')
     READ(5,2010) G
2010 FORMAT(A1)
3500 IF (G.EQ.'Y'.ÓR.G.EQ.'y') THEN
     WRITE(6,2020)
2020 FORMAT(8X, ENTER ANGLE BETWEEN MAG FIELD AND gz-AXIS')
     READ(5,2030) TH
2030 FORMAT(F5.2)
     WRITE(6,2040)
2040 FORMAT(5X, ENTER MAGNETIC FIELD VALUE')
     READ(5,2050) MF
2050 FORMAT(F7.2)
     TH = TH * 0.01745
     STH = SIN(TH)
     CTH=COS(TH)
     VN = 4.257708E - 3*MF
     H(3) = CTH
```

```
DO 2100 I = 1.360
        ANG = I * 0.01745
       H(1) = STH*COS(ANG)
       H(2) = STH*SIN(ANG)
           DO 2200 J = 1.3
             DO 2200 K = 1.3
                 LH(J) = H(K) *EGVC(K,J) + LH(J)
             CONTINUE
2200
           DO 2300 J = 1.3
                 AF = EGVL(J)*LH(J)**2+AF
                 LH(J) = 0.0
           CONTINUÉ
2300
     PC(I) = VN + (AF/2)
     MC(I) = VN-(AF/2)
      WRITE(11,2350) PC(I),I,MC(I),I
2350 FORMAT(1X,2(F11.6,I6))
     AF = 0.0
2100 CONTINUE
     LPC = PC(1)
     SPC = PC(1)
     LMC = MC(1)
     SMC = MC(1)
     DO 2400 I = 2.360
       IF (PC(I).GT.LPC) LPC=PC(I)
       IF (PC(I).LT.SPC)' SPC=PC(I)
       IF (MC(I).GT.LMC) LMC=MC(I)
       IF (MC(I).LT.SMC) SMC=MC(I)
2400
     CONTINUÉ
      WRITE(12,2410)
2410 FORMAT(/,10X,'ENDOR COUPLINGS')
      WRITE(12.2420)
     FORMAT(/,1X,'POSITIVE COUPLING')
2420
     WRITE(12,2430) LPC,SPC
2430
    FORMAT(/,1X,'LARGE COUPLING = ',F11.6,'SMALL COUPLING =
     '.F11.6)
     WRITE(12,2440)
2440 FORMAT(/,1X,'NEGATIVE COUPLING')
     WRITE(12,2450) LMC,SMC
2450
    FORMAT(/,1X,'LARGE COUPLING = ',F11.6,'SMALL COUPLING =
     '.F11.6)
     WRITE(12,2455) VN
2455 FORMAT(/,/,1X,'FREE PROTON RESONANCE = ',F6.3)
     TH = TH/0.01745
     WRITE(12,2460) MF.TH
2460 FORMAT(/,/,1X,'MAGNETIC FIELD= ',F7.2,' ANGLE THETA=',F5.2)
     WRITE(6,3100)
3100 FORMAT(6X. CALCULATE ANOTHER SET OF ENDOR
     FREQUENCIES')
     READ(5,3150) G
3150 FORMAT(A1)
     GOTO 3500
     ENDIF
C
     RETURN TO TOP TO RERUN PROGRAM
```

```
C
1570 WRITE(6,1580)
1580 FORMAT(/,' DO YOU WISH TO ENTER A NEW SET OF DATA
[Y/N]')
READ(5,1590) F
1590 FORMAT(A1)
       IF (F.EQ.'Y'.ÓR.F.EQ.'y') then
       DO 1620 J = 1,3
              HCR(J) = 0.0
              SDR(J) = 0.0
       DO 1610 \text{ K} = 1.3
               GCR(J,K) = 0.0
               A(J,K) = 0.0

AS(J,K) = 0.0
1610
              CONTÍNUE
1620 CONTINUE
       GOTO 2000
       ELSE
         GOTO 1700
       ENDIF
1700 STOP
       END
```



## **BIBLIOGRAPHY**

- Guss, J.M.: Freeman H.C., J. Mol. Biol., 1983, 169, 521-563 1)
- Adman, E.T., "Metalloproteins Part 1: Metal proteins with redox roles": 2) Pauline Harrison Ed.; Verlog Chemie: Weinheim, Germany, 1985; pp1-48
- "Copper Proteins and Copper Enzymes": Rene Lontie Ed.: CRC Press, Baco 3) Raton, FL, 1984, pp 184
- Adman, E.T.; Jensen, L.H., Isr. J. Chem., 1981, 21, 8-12
- 4) 5) Norris, G.E.; Anderson, B.F.; Baker, E.N., J. Am. Chem.Soc., 1986, 108, 2784-2785
- 6) Solomon, E.I., Comments Inorg. Chem., 1984, 3, 227-320
- Markley, J.K.; Ulrich, E.L.; Berg, S.P.; Krogmann, D.W., Biochemistry, 1975, 7) 14, 4428-4433
- 8) Solomon, E.I.; Clendening, P.J.; Gray, H.B.; Grunthaner, F.J., J. Am. Chem. Soc., 1975, 97, 3878-3879
- 9) Solomon, E.I.; Hare, J.W.; Gray, H.B., Proc. Natl. Acad. Sci. USA, 1976, 73, 1389-1393
- 10) Hathaway, B.J.; Tomlinson, A.A.G., Coord. Chem. Rev., 1970, 5, 1-46
- 11) Bryce, G.F., J. Phys. Chem., 1966, 70, 3549-3555
- Corrigan, M.F.; Murray, K.S.; West, B.O.; Pilbrow, J.R., Aust. J. Chem, 1977, 12) 30,2455-2462
- Huheey, J. "Inorganic Chemistry Principles of Structure and Reactivity"; 13) Harper & Row: New York, 1983: pp384-385
- 14) Fee, J.A., "Structure and Bonding"; Springer Verlag: NewYork, 1975, 23, 1-60
- Hatfield, W.E.; Jones, E.R.Jr., Inorg. Chem., 1970, 6,1502-1508 15)
- 16) Wood, J.S., J. Chem. Soc. A, 1969, 1582-1590
- Slade, R.C.; Tomlinson, A.A.G.; Hathaway, B.J.; Billing, D.E., J.Chem. Soc. 17) A, 1968, 61-69
- Barbucci, R.; Bencini, A.; Gatteschi, D., Inorg, Chem., 1977, 16,2117-2221 18)

- 19) Solomon, E.I.; Hare, J.W.; Dooley, D.M.; Dawson, J.H.; Stephens, P.J.; Gray, H.B., J. Am. Chem. Soc., 1980, 102, 168-178
- 20) Iwaizumi, M.; Kudo, T.; Kita, S., Inorg. Chem., 1986, 25, 1546-1550
- 21) Penfield, K.W.; Gewirth, A.A.; Solomon, E.I., J. Am. Chem. Soc., 1985, 107, 4519-4529
- "Copper Proteins and Copper Enzymes"; Rene Lontie Ed., CRC Press, Boca Roton, FL, 1984, pp 94
- 23) Tullius, P.F.; Hodgson, K.O., Proc. Natl. Acad. Sci. USA, 1978, 75, 4069-4073
- 24) Tullius, T.D., Ph.D. Thesis, Stanford University, 1979
- Colman, P.M.; Freeman, H.C.; Guss, J.M.; Murata, M.; Norris, V.A.; Ramshaw, J.A.M.; Venkatappa, M.P., Nature, 1978, 272, 319-324
- 26) Garret, T.P.J.; Clingeleffer, D.J.; Guss, J.M.; Rogers, S.J.; Freeman, H.C., J. Biol. Chem., 1984, 259, 2822-2825
- 27) Guss, J.M.; Harrowell, M.M.; Norris, V.A.; Freeman, H.C., J. Mol. Biol., 1986, 192, 361-387
- 28) Church, W.B.; Guss, J.M.; Potter, J.P.; Freeman, H.C., J. Biol. Chem., 1986, 261, 234-237
- 29) Engeseth, H.R.; McMillin, D.R.; Otvos, J.D., J. Biol. Chem., 1984, 259, 4822-4826
- 30) Armstrong, F.A.; Driscoll, P.C.; Hill, H.A.O.; Redfield, C., J. Inorg. Biochem., 1986,28,171-180
- 31) Chazin, W.J.: Wright, P.E., J. Mol. Biol., 1988, 202, 623-636
- 32) Wuthrich, K. "NMR of Proteins and Nucleic Acids"; John Wiley and Sons: NewYork, 1986
- 33) Driscoll, P.C.; Hill, H.A.O.; Redfield, C., Eur. J. Biochem, 1987, 170, 279-292
- 34) Mustafi, D.; Makinen, M., Inorg. Chem., 1988, 27, 3360-3368
- 35) Kevan, L.; Kispert, L. "Electron Spin Double Resonance Spectroscopy"; John Wiley and Sons: New York, 1976, 1-57
- 36) Kirste, B.; van Willigen, H., J. Phys. Chem., 1983, 87, 781-788
- 37) Yim, M.B.; Makinen, M.W., J. Mag. Res., 1986, 70, 89-105
- 38) Roberts, J.E.; Cline, J.F.; Lum, V.; Freeman, H.; Gray, H.B.; Peisach, J.; Reinhammer, B.; Hoffman, B.M., J. Am. Chem. Soc., 1984, 106, 5324-5330
- 39) Roberts, J.E.; Brown, T.G.; Hoffman, B.M., Peisach, J., J. Am. Chem. Soc., 1980, 102, 825-829

- 40) Abragam, A.; Bleaney, B.; "Electron Paramagnetic Resonance of Transition Ions", Dover Publications, New York, 1970, pp 27
- 41) Atkins, P.W.; Symons, M.C.R. "The Structure of Inorganic Radicals"; Elsevier: Amsterdam, 1967; pp 268-270
- 42) Gordy, W. "Theory and Application of Electron Spin Resonance"; John Wiley and Sons: New York, 1980; pp 48-68
- 43) Wells, G.B.; Makinen, M.W., J. Am. Chem. Soc., 1988, 110, 6343-6352
- 44) Baker, G.J.: Raynor, J.B., J. Chem. Soc. Dalton Trans., 1986, 2663-2667
- The program PROTIN was used in the laboratory of Dr. A. Tulinsky, Dept. of chemistry, Michigan State University, East Lansing, MI
- 46) Kerr, K.A.; Ashmore, J.P., Acta. Cryst., 1975, B31, 2022-2026
- 47) Fuess, H.; Hohlwein, D.; Mason, S.A., Acta. Cryst., 1977, B33, 654-659
- 48) Penfield, K.W.; Gay, R.R.; Himmelwright, R.S.; Eickman, N.C.; Norris, V.A.; Freeman, H.C.; Solomon, E.I., J. Am. Chem. Soc., 1981, 103, 4382-4388
- 49) IMSL Fortran Subroutines, IMSL Software Systems, Houston Tx, USA
- 50) Kevan, L., and Kispert, L., in "Electron Spin Double Resonance Spectroscopy", John Wiley & Sons, New York, 1976, pp 240
- 51) Hurst, G.; Kraft, K.; Kreilick, R., J. Magn. Reson., 1982, 49,159-165
- 52) Nilges, M.J., PH. D. thesis, University of Illinois, 1979
- 53) Groeneveld, C.M.; Aasa, R.; Reinhammer, B.; Canters, G.W., J. Inorg. Biochem., 1987, 31, 143-154
- 54) Malkin, R.; Bearden, A.J., BBA, 1973, 292, 169-185
- 55) Scawan, M.D.; Ramshaw, J.A.M.; Boulter, D., Biochem J., 1975, 147, 343-349
- 56) Wells, J.W.; Box, H.C., J. Chem. Phys., 1968, 48, 2542-2546
- 57) Clough, S.; Poldy, F., J. Chem. Phys., 1969, 51, 2076-2084
- 58) O'Malley, P.J.; Babcock, G.T., J. Am. Chem. Soc., 1986, 108, 3995-4001
- 59) Bender, C.J.; Sahlin, M.; Babcock, G.T.; Barry, B.A., J. Am. Chem. Soc., 1989, 111, 8076-8083
- 60) Ellefson, W.L.; Ulrich, E.A.; Krogman, D.W., Methods in Enzymology, 1980, 69, 223-230
- 61) Negritiu, I.; De Brouwer, D.; Dirks, R.; Jacobs, M., Mol. Gen. Genet., 1985, 199, 330-337

- 62) Currier, T.C.; Haury, J.F.; Wolk, C.P., J. Bacteriol., 1977, 129, 1556-1562
- 63) Farver, O.; Shahak, Y.; Pecht, I., Biochemistry, 1982, 21, 1885-1891
- 64) Burkey, K.O.; Gross, E.L.; Biochemistry, 1982, 21, 5886-5893

HICHIGAN STATE UNIV. LIBRARIES
31293009108568